



Numerical study on the climatic effect of the lake clusters over Tibetan Plateau in summer

Yang Wu^{1,2} · Anning Huang^{1,2} · Ben Yang^{1,2} · Guangtao Dong³ · Lijuan Wen⁴ · Lazhu⁵ · Zhiqi Zhang^{1,2} · Zhipeng Fu^{1,2} · Xueyan Zhu^{1,2} · Xindan Zhang^{1,2} · Shuxin Cai^{1,2}

Received: 28 November 2018 / Accepted: 13 June 2019 / Published online: 21 June 2019
© The Author(s) 2019

Abstract

The weather research and forecasting model including a one-dimensional thermal diffusion lake model is adopted to investigate the summer climatic effect of the lake clusters over Tibetan Plateau (TP) during 2008–2014 based on two experiments with and without the lakes. Overall, the model can reasonably reproduce the daily variations of lake surface temperature and the spatial patterns of 2 m air temperature (T_{2m}) and precipitation over TP during summer. Sensitivity results show that the effects of TP lakes on the over-lake T_{2m} and precipitation exhibit distinctive seasonal and diurnal features and strong space dependence. Generally, the TP lakes tend to cool the local T_{2m} and enhance the precipitation over the lake and surrounding areas. With the summer advances, the cooling effect of TP lakes weakens while the lake-induced enhancement of precipitation becomes more evident. During daytime, the TP lakes decrease the T_{2m} and suppress the short-duration (≤ 6 h) rainfall in afternoon. However, the TP lakes increase the T_{2m} and strengthen the convective rainfall over the lake and surrounding areas by simultaneously enhancing both short and long-duration (> 6 h) precipitation during nighttime. The lakes over the southeastern central TP (CTP) lead to slight warming and pronounced precipitation increases, while the other lakes in CTP mainly cause significant cooling and suppressed precipitation. Such opposite effects are mainly because the lakes over the western and northeastern CTP hardly produce nighttime warming and the associated circulation changes favorable for the convective precipitation as found over the southeastern CTP, suggesting that the climate effects of TP lakes may be modulated by the lake intrinsic features, local terrain distributions, and background atmospheric circulations.

1 Introduction

The lake-air interaction, a considerable issue of the reciprocal effect between the atmosphere and the underlying surface, plays a significant role in modulating the weather and climate at local to regional scales (Adrian et al. 2009). Compared to the surrounding land or vegetation surface, lakes are important moisture sources for low-level atmosphere and characterized by unique physical properties, i.e. low albedo, small surface roughness and high thermal inertia, which can directly alter the surface thermal conditions and the water and energy balances (Ma et al. 2014; Nordbo et al. 2011; Krinner 2003; Stepanenko et al. 2014). As a result, the regions with high lake concentrations show distinctive spatiotemporal features of temperature, precipitation and wind fields (Curtarelli et al. 2014; Thiery et al. 2014). This is particularly the case in the Tibetan Plateau (TP), where there exist more than 1200 lakes with an individual surface area above 1 km². The total lake area over the TP exceeds 40,000 km², which accounts for around 52% of the

✉ Anning Huang
anhuang@nju.edu.cn

✉ Ben Yang
byang@nju.edu.cn

¹ CMA-NJU Joint Laboratory for Climate Prediction Studies, School of Atmospheric Sciences, Nanjing University, No. 163 Xianlin Avenue, Nanjing, Jiangsu 210023, China

² State Key Laboratory of Severe Weather and Joint Center for Atmospheric Radar Research of CMA/NJU, Beijing, China

³ Climate Center, Shanghai Meteorological Bureau, Shanghai, China

⁴ Key Laboratory of Land Surface Process and Climate Change in Cold and Arid Regions, Chinese Academy of Sciences, Lanzhou 730000, China

⁵ Key Laboratory of Tibetan Environment Changes and Land Surface Processes, Institute of Tibetan Plateau Research, Chinese Academy of Sciences, Beijing 100101, China

total lake coverage in China (Zhang et al. 2014). Because of the distinct climate over the TP and its important role in the earth system, the variations in the physical and biochemical properties of the TP lake clusters can lead to dramatic environmental and climate changes (Lei et al. 2014; Phan et al. 2012; Song et al. 2014; Verburga and Hecky 2009). Hence, revealing the climatic effects of the TP lake clusters is not only important for understanding the regional changes in hydrological cycle and energy budgets, but also helpful to evaluate and improve the performances of the lake-air coupled climate model (Dutra et al. 2010; Mironov et al. 2010; Xu et al. 2016).

During the past several years, many researchers have paid lots of attention to the lake-air interactions at various spatiotemporal scales (Bonan 1995; Hostetler et al. 1993, 1994; Long et al. 2007; Lofgren 1997). Results have shown that as one of the typical land categories, inland lakes can lead to the spatiotemporal heterogeneity of surface energy budgets, which can further affect the atmospheric circulations and the regional weather and climate (Alcott et al. 2012; Bartunkova et al. 2014; Yeager et al. 2013; Gu et al. 2016; Xiao et al. 2016). For example, due to the large thermal inertia, the presence of lakes delays the autumn/nighttime (spring/daytime) cooling (warming) and therefore dampens the diurnal and seasonal variations of low-level temperature in the Canadian Shield (Gula and Peltier 2012; Martynov et al. 2012; Notaro et al. 2013). Additionally, the warmer (cooler) lake surfaces during winter/nighttime (summer/daytime) tend to generate a convergent (divergent) flow due to the lake-land thermal gradient, which enhances (suppress) the over-lake convective development and cloud formation (Ruthrich et al. 2015; Zhao et al. 2012). Such lake effects can lead to increases of precipitation and heavy snowfall during winter especially in the downwind regions (Pereira and Muscato 2013; Theeuwes et al. 2010; Vavrus et al. 2013). Different from the climatic effect of the Great Lakes, Samuelsson et al. (2010) found that the lakes in the northern Europe with temperate climate act to increase T_{2m} for all seasons and enhance the convective precipitation during late summer and early autumn. In contrast, the Lake Victoria in the tropic results in lower air temperature and enhanced rainfall throughout the entire year (Williams et al. 2015). Additionally, contrast to the pronounced downwind influence of the Great Lakes on the rainfall, the lake-induced precipitation changes in the African Great Lakes can hardly exceed the lake shores (Thiery et al. 2015).

Overall, the lake effects are found to be prominent in lake-abundant regions but exhibit distinctive diurnal and seasonal features in different regions, depending on the lake intrinsic natures, surrounding topography and background atmospheric circulations (Argent et al. 2015; Subin et al. 2012; Wen et al. 2015a). Compared to the temperate-zone or tropical lakes, the lakes over the TP can transfer vast heat and water fluxes directly to the middle troposphere, which can

further interact with the large scale tropical and extratropical systems during the boreal summer (Yanai et al. 1992; Wu et al. 2012; Xue et al. 2017). Hence, it is imperative to have a comprehensive understanding of the lake-air interactions and the climatic effects of the lake clusters over TP.

Recently, with the gradual development of field measurement techniques and computer performances, more observations and simulations have been conducted to study the lake properties and the lake-air interactions over the alpine and cold regions, such as over the TP (Biermann et al. 2014; Gerken et al. 2013; Lazhu et al. 2016; Liao et al. 2013; Lu et al. 2017; Wang et al. 2010, 2017; Zhu et al. 2017). Based on the multi-source sounding data at Lake Nam Co and the MM5 model, Lv et al. (2008) revealed that the variations of heat fluxes induced by the lake-land thermal contrast is an important reason for the dramatic changes of the local circulations and mesoscale weather. Specifically, at the diurnal scale, Lake Nam Co leads to higher (lower) air temperature and enhanced (suppressed) convection during nighttime (daytime). The annual mean over-lake evaporation is more than two times of that from the surrounding land, with the lake-land differences in moisture and heat fluxes reaching their annual peaks in the post-monsoon period (Haginoya et al. 2009; Xu et al. 2011). Gerken et al. (2013) further demonstrated that as the Lake Nam Co is situated at the foot of the Nyainqentanglha, the effect of the lake-land breeze can be superimposed by that of the mountain-valley wind in modulating the moist and deep convection. In addition to the Lake Nam Co, the lake-air interactions have also been investigated over some other lakes in the TP, such as the Qinghai Lake (Lv et al. 2007), the Lake Tangra Yamco (Wang et al. 2010), the Ngoring and Gyaring Lake (Li et al. 2015; Wen et al. 2015b). However, previous modeling studies mainly focused on limited periods and set prescribed or the extrapolated sea surface temperature as lake surface temperature to force the atmosphere model, which may not be suitable for simulating the lake effects on the surface fluxes, temperature, and precipitation at climate scales. Moreover, previous studies mainly explored the local effect of some individual lakes. It is still unclear how the cluster effects of the widespread lakes in the TP can affect the climate at local to regional scales. In this study, a fully coupled air-lake model (WRF-Lake, Gu et al. 2015; Skamarock et al. 2008) is applied to more realistically represent the lake-air interactions over the TP, which would be helpful to deepen our understanding of the lake climatic effects over the TP.

The rest of this paper is organized as follows: a brief description of the datasets, the regional climate model, and the methods are given in Sect. 2. In Sect. 3, we firstly evaluate the model performances in simulating the lake surface temperature, precipitation and T_{2m} . The climatic effect of the TP lakes is revealed and discussed in Sect. 4. Finally, the conclusions and discussions are given in Sect. 5.

2 Datasets, model description and experimental design, and methodology

2.1 Datasets

The datasets used in current study are listed as follows: (1) the National Centers for Environmental Prediction-Global Final Analysis (NCEP-FNL) data with a $1^\circ \times 1^\circ$ grid spacing and 6-h interval (<https://rda.ucar.edu/datasets/ds083.2/>, NCEP/NOAA 2000); (2) the daily, $0.5^\circ \times 0.5^\circ$ real-time global sea surface temperature dataset (ftp://polar.ncep.noaa.gov/pub/history/sst/rtg_low_res/, Thiébaux et al. 2003); (3) the Moderate Resolution Imaging Spectroradiometer (MODIS) land-use categories with a horizontal resolution of 10 arc seconds (Friedl et al. 2010); (4) the global lake database version 2 (GLDBv2) including the lake location and depth with the horizontal resolution of 1 km developed by Kourzeneva (2010), Kourzeneva et al. (2012) and Choulga et al. (2014), which are available at <https://www.flake.igb-berlin.de/ep-data.shtml>; (5) the field observed depth data of Lake Nam Co provided by Wang et al. (2009); (6) the global lake surface water temperatures (LSWT) during 1995–2011 provided by the Along-Track Scanning Radiometers (ATSR) Reprocessing for Climate (https://www.laketemp.net/home/dataF/ARC_Lake_V3.0, MacCallum and Merchant 2012); (7) the T_{2m} data from the 6-h, $0.25^\circ \times 0.25^\circ$ ERA-Interim reanalysis (Simmons et al. 2007) during 2008–2014 which are available at <https://apps.ecmwf.int/datasets/data/interim-full-daily>; (8) the rainfall data of the Tropical Rainfall Measuring Mission 3B42 (TRMM3B42) version 7 (Huffman et al. 2007), which are available at <ftp://disc2.nascom.nasa.gov/data/TRMM/Gridded>. The TRMM3B42 dataset covers a relatively wide global latitude band of 50°S – 50°N with a high spatial resolution of 0.25° and temporal resolution of 3 h. Due to the plentiful calibrations against Global Precipitation Climatology Center monthly gauge records, TRMM3B42 dataset has been identified to agree well with the gauge observations in the overall spatiotemporal variations of precipitation over China (Huang et al. 2016; Maussion et al. 2013).

2.2 Model description and experimental design

The advanced research WRF (WRF-ARW V3.8.1, Skamarock et al. 2008), a fully compressible and non-hydrostatic model with multiple parameterization schemes and flexible resolutions, is employed in this study. The lake model component in the WRF used here is the Community Land Model version 4.5 lake model (Oleson et al. 2013), which

mainly origins from the basic concepts of the Hostetler lake model (Hostetler et al. 1993) and further developed by Subin et al. (2012) and Gu et al. (2015). It is a one-dimensional mass and energy balance model including ten lake water layers, ten soil layers in the lake bottom and up to five snow layers on the lake ice. In this study, we intend to use the air-lake coupled regional climate model for a better representation of lake physical processes and lake-air interactions, such as the turbulent fluxes of energy, moisture, and momentum between the lake surface and the lower atmosphere. Some other key physical options adopted in this study are as follows: the Noah land surface model (Mitchell et al. 2005), the WRF Single-Moment 6-class microphysics scheme (Hong et al. 2006b), the Grell-Devenyi ensemble cumulus scheme (Grell and Devenyi 2002), the Yonsei University planetary boundary layer scheme (Hong et al. 2006a), the Dudhia shortwave radiation scheme (Dudhia 1989), and the rapid radiative transfer model for longwave radiations (Mlawer et al. 1997).

The model encompasses two two-way nested domains with the horizontal resolutions of 30 km in Domain 1 and 10 km in Domain 2 and 31 sigma levels with its top at 50 hPa (Fig. 1a). Following Gao et al. (2016), the large mother domain (Domain 1), which covers most Asia continental areas, parts of the northern Indian Ocean and the northwestern Pacific Ocean, is designed to capture the interactions between the external large-scale environment and the regional weather systems over the TP in the nested domain (Fig. 1a). The inner domain (Domain 2) in Fig. 1a covers almost the whole TP. Specifically, the staggered grid points for both domains are 220×160 and 259×172 in the east–west and north–south directions, respectively. The land surface types on each model grid in the model domains are derived from the MODIS land-use categories. The lake fraction (the ratio of sub-grid lake area to the grid area at each model grid) and lake depth (mean sub-grid lake depth at each model grid) on each domain grid are provided by the GLDBv2 dataset (Choulga et al. 2014). Because the GLDBv2 dataset do not contain the depth of Lake Nam Co, the actual lake depth is updated by the field observed bathymetry data provided by Wang et al. (2009) (Fig. 1b). The lake fraction and depth in domain 2 are shown in Fig. 1c, d, respectively. It is noted that the lakes widely spread over the central TP (CTP) with the lake fraction ranging from 0.1 to 1.0. Some large lakes such as Lake Nam Co, Lake Siling Co, and Qinghai Lake can be explicitly resolved by the model with the horizontal resolution of 10 km. The model initial and lateral boundary conditions are generated from the NCEP-FNL data (NCEP 2000). The sea surface temperature is prescribed by using the daily, $0.5^\circ \times 0.5^\circ$ real-time global sea surface temperature dataset (Thiébaux et al. 2003).

Based on the common model configurations, we design two experiments with and without TP lakes, hereafter

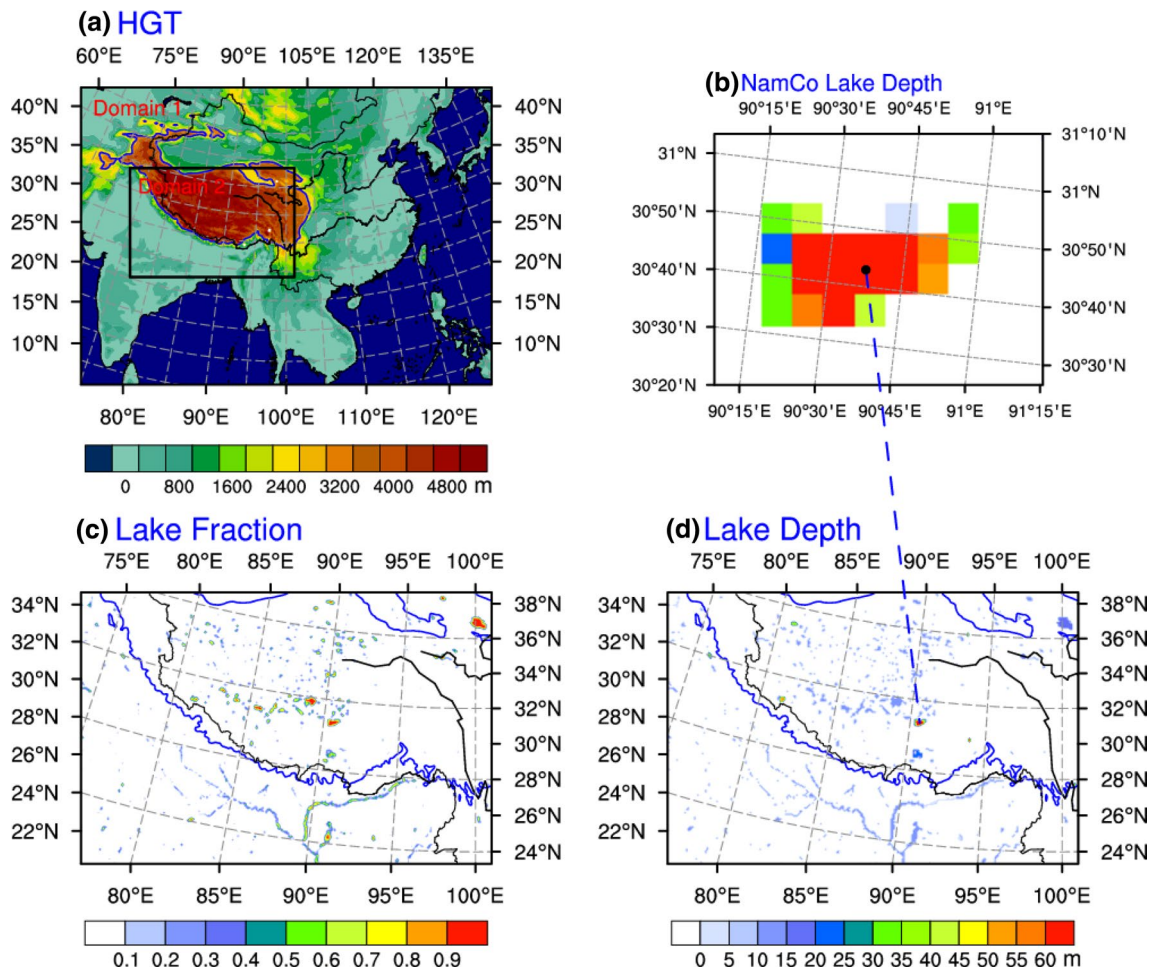


Fig. 1 **a** Geographic locations and terrain height of the two domains adopted in the WRF-Lake model. **b** The spatial distributions of the lake depth in Lake Nam Co. **c** The sub-grid lake fraction and **d** mean

lake depth in Domain 2. In **a**, **c**, and **d**, the blue curves with an altitude of 3000 m outline the TP and the thick black lines denote the Yangtze River and the Yellow River

abbreviated as CTRL and NOL, respectively. The real lakes over the TP are included in the CTRL experiment. In the NOL experiment, all the TP lakes are replaced by the representative land-use category in each model grid. In each experiment, the model runs start on 20th May and end on 31st August for each year from 2008 to 2014. The first 12 days are for spin-up and only the summer results (June–July–August, JJA) are applied for the analysis. The comparisons between the CTRL and NOL simulations are used to quantify the TP lake effects on the climate at local to regional scales.

2.3 Methodology

All the observation data are first interpolated onto the model grid points using the simple inverse distance weighting method (Shepard 1968). Following Huang et al. (2016), we utilize three common statistics, i.e. the temporal/spatial correlation coefficient (TC/PC, Eq. 1), the root-mean-square

error (RMSE, Eq. 2), the Taylor score (TS, Eq. 3) to evaluate the model performances. Given the sharp gradients and singularities in the model buffer zones, ten grid points in the domain lateral boundaries are excluded when calculating all the above statistics (Davies and Turner 1977; Thiery et al. 2015). The equations for the statistical measures are given by:

$$TC/PC = \frac{\sum_{i=1}^N (M_i - \bar{M})(O_i - \bar{O})}{\sqrt{\sum_{i=1}^N (M_i - \bar{M})^2} \sqrt{\sum_{i=1}^N (O_i - \bar{O})^2}} \quad (1)$$

$$RMSE = \sqrt{\frac{1}{N} \sum_{i=1}^N (M_i - O_i)^2} \quad (2)$$

$$TS = \frac{4(1 + PC)}{(\sigma + 1/\sigma)^2(1 + PC_0)} \quad (3)$$

$$\left[\sigma = \sqrt{\frac{1}{N} \sum_{i=1}^N (M_i - \bar{M})^2} / \sqrt{\frac{1}{N} \sum_{i=1}^N (O_i - \bar{O})^2} \right] \quad (4)$$

where $M_i(O_i)$ is the model simulations (observations) at N temporal or spatial points, and $\bar{M}(\bar{O})$ presents the averaged value of model simulations (observations) over the N points. TC (PC) is adopted to describe the temporal (spatial) similarity between the simulations and observations, and RMSE is used to quantify the deviation of the simulations from the observations (Su et al. 2013). High TC (PC) indicates large similarity in temporal variation (spatial distribution) between the simulations and observations; while low RMSE indicates that the simulations have more agreement with the observations in quantity. TS is proposed by Taylor (2001) to quantify how simulations match observations in terms of both spatial pattern and magnitude. σ is the spatial standard deviation of the model simulations normalized by that of the observations. PC_0 is the achievable maximum pattern correlation (set as 1). As revealed by Eq. (3), TS ranges from 0 to 1 and a larger TS indicates better model performance.

Following Yu et al. (2007), the number of hours between the start and the end of a rainfall event without any intermittence (i.e. during which the precipitation is less than 0.1 mm h^{-1}) are regarded as the duration time. The short-duration ($\leq 6 \text{ h}$) and long-duration ($> 6 \text{ h}$) rainfall events are picked out based on the criterion mentioned above. Then we further calculate the precipitation amount (PA, the accumulated measurable precipitation divided by the total hours in summer), frequency (PF, the percentage of total precipitating hours with the measurable precipitation $\geq 0.1 \text{ mm h}^{-1}$ to the total hours in summer), and intensity (PI, the accumulated measurable precipitation averaged over the total precipitating hours) for rainfall events with different duration times (Zhou et al. 2008; Wu et al. 2017) during 2008–2014.

To estimate the contribution of each surface heat component to the lake-induced surface temperature change, we adopt the surface heat balance decomposition method suggested by Thiery et al. (2015) based on the surface heat balance equation:

$$[\varepsilon\sigma T_s^4 = (1 - \alpha)SW_{in} + LW_{in} - SHF - LHF - G] \quad (5)$$

where, ε is the surface emissivity, $\sigma = 5.67 \times 10^{-8} \text{ Wm}^{-2} \text{ K}^{-4}$ is the Stefan–Boltzmann constant, T_s is the surface temperature, α is the surface albedo with respect to the incoming shortwave radiation SW_{in} (positive downwards). LW_{in} is the downward incoming longwave radiation (positive downwards). SHF and LHF (positive upwards) are the turbulent fluxes of sensible and latent heat, G is the ground heat flux (positive upwards), which is the combined subsurface heat storage and conductive heat fluxes. Neglecting the high-order terms, the first order derivative of the net changes in

outgoing longwave radiation at surface (i.e. left hand side in Eq. 5) can be expressed by $4\varepsilon\sigma T_s^3 \delta T_s$. Hence, the δT_s can be derived by solving the total derivative of Eq. 5 as follows:

$$\delta T_s = \frac{1}{4\varepsilon\sigma T_s^3} [-SW_{in}\delta\alpha + (1 - \alpha)\delta SW_{in} + \delta LW_{in} - \delta LHF - \delta SHF - \delta G - \sigma T_s^4 \delta\varepsilon] \quad (6)$$

According to Eq. 6, it is obvious that the net lake effect on T_s is decomposed a posteriori and contributed by the direct forcing changes related to different surface types (such as surface albedo, evapotranspiration, surface roughness lengths and surface emissivity) and indirect forcing changes due to atmospheric feedbacks (such as cloud radiative feedbacks or surface layer stability changes) (Thiery et al. 2015). Most terms of Eq. 6 can be computed from the mean of the 3 h differences between the CTRL and NOL simulations.

To describe the atmospheric stability, we utilize the equivalent potential temperature θ_e given by:

$$\theta_e = \left(T + \frac{L_v q_v}{C_p} \right) (P_0/P)^{\frac{R}{C_p}} \quad (7)$$

where T is the air temperature, L_v is the latent heat of evaporation ($2.5 \times 10^6 \text{ J kg}^{-1}$), q_v is the specific humidity, C_p is the specific heat capacity of air at constant pressure ($1005 \text{ J kg}^{-1} \text{ K}^{-1}$), P_0 is the standard atmospheric pressure ($1 \times 10^5 \text{ Pa}$), and P is the air pressure.

3 Model evaluation

3.1 Lake surface water temperature

To validate the model behavior in reproducing lake surface water temperature (LSWT), we compare the simulations of the CTRL experiment with the ARC_Lake data for the sub-seasonal variations of the LSWT over the Qinghai Lake, which is the largest lake in the TP with an area more than 4500 km^2 and a mean depth of 21 m. Figure 2 shows that the WRF-Lake model can reasonably reproduce the day-to-day variations of the LSWT of the Qinghai Lake in summer but exhibits a slight cold bias during the post-monsoon period. The TC, bias, and RMSE between the simulated and observed LWST averaged over 2008–2011 are 0.98, $-0.435 \text{ }^\circ\text{C}$, and $0.85 \text{ }^\circ\text{C}$, respectively (Fig. 2a). This reasonable simulation is primarily due to the effective calibrations of eddy diffusivity conducted by many previous researchers, which improve the capability of Hostetler-based models in simulating the thermodynamics especially in shallow lakes (Subin et al. 2012; Gu et al. 2015). For the Lake Nam Co with the mean depth exceeding 40 m and the maximal depth

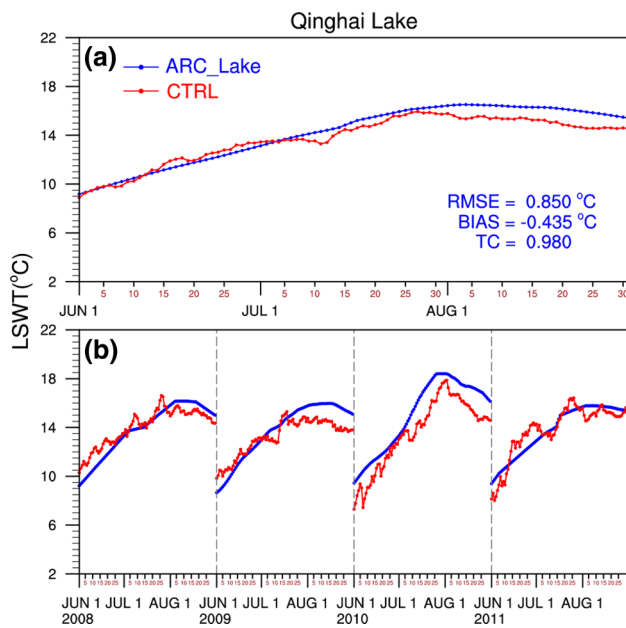


Fig. 2 The daily ARC_Lake observed (blue lines) and CTRL simulated (red lines) lake surface temperature **a** averaged over 2008–2011 and **b** in each year of 2008–2011 for the Qinghai Lake

over 120 m (Lazhu et al. 2016; Wang et al. 2009) (Fig. 1d), the simulated LWST (figures not shown) exhibit a characteristic of stronger warming in early summer compared to the observations. Similar biases have also been reported by

Xiao et al. (2016) when applying the WRF-Lake model to simulate the thermal features of the deep Laurentian Lakes. The TC, bias, and RMSE between the simulations and observations in the Lake Nam Co are 0.963, 1.363 °C, and 1.276 °C, respectively, indicating that the representation of deep lake processes remains to be improved in the future studies. However, based on the global lake depth data from Choulga et al. (2014), most lakes over the TP belong to shallow lakes, which means the present WRF-Lake model with reliable capability in capturing the LSWT variations and the corresponding energy fluxes in shallow lakes is adequately suitable for the further lake-effect studies.

3.2 Precipitation and 2 m air temperature

During boreal summer, TP serves as a huge, elevated heat source to the middle troposphere (Yanai et al. 1992; Wu et al. 2012; Xue et al. 2017). The powerful sensible heat pump effect of the TP can drive the low-level moisture advection from Bay of Bengal to the Indian peninsula, generating the large rainfall center with the intensity approximately 10 mm day^{-1} over the Ganges Plain (Fig. 3a). One branch of the moist flow is blocked and redirected northwest by the Himalayas and the other branch blows northeastward into the southeastern TP through the deep canyons therein (Maussion et al. 2013; Zhang et al. 2017), which lead to the formation of strong orographic rainfall belt with the maximal intensity exceeding 25 mm day^{-1}

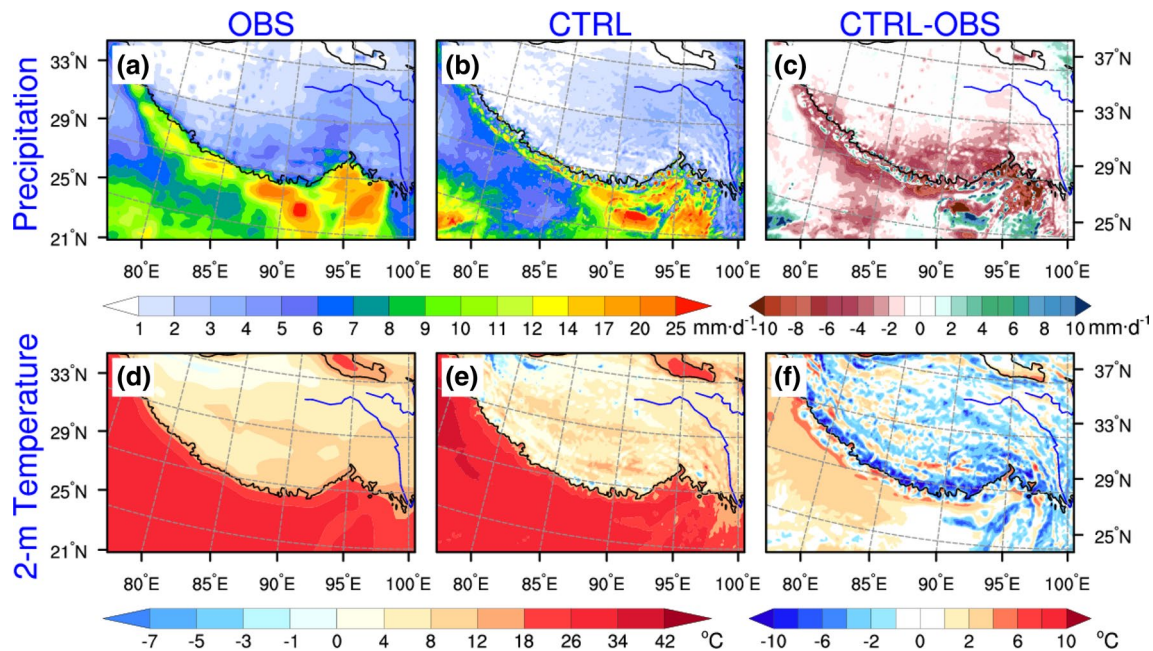


Fig. 3 The summer mean observed (**a**, **d**) and CTRL simulated (**b**, **e**) precipitation and 2 m air temperature and the differences (**c**, **f**) between CTRL simulations and the observations over the nested

domain averaged over 2008–2014. The black curves with an altitude of 3000 m outline the TP, while the blue lines denote the upstream of the Yangtze River and the Yellow River

Table 1 The verification statistics between the simulations and observations for the precipitation and 2 m air temperature over domain 1 (D01) and domain 2 (D02)

Variables	Domains	Statistics		
		PC	TS	RMSE
Precipitation	D01	0.81	0.86	3.74 mm day ⁻¹
	D02	0.81	0.90	3.24 mm day ⁻¹
T _{2m}	D01	0.98	0.97	2.81 °C
	D02	0.98	0.98	1.63 °C

The PC, TS, and RMSE represent the pattern correlation, Taylor score, and root-mean-square-error, respectively

along the south edge of Himalayas (Fig. 3a). As the westerly jet axis is located over the northern TP during boreal summer, the precipitation over the TP is mainly modulated by the summer monsoon circulations and exhibit a decreasing trend from southeast to northwest (Fig. 3a). As shown in Fig. 3a–c, WRF-Lake model well reproduces the spatial pattern of the summer precipitation but fails to simulate the magnitude of the rainfall distribution, especially among the steep Himalayas, which has been a long-standing issue in many climate models (Yu et al. 2015; Zhu et al. 2017). Due to the more detailed and realistic descriptions of topography contrast and landuse categories, our high-resolution model results have a relative bias of 25.7% in the summer precipitation simulations, outperforming those from CMIP5 models (Su et al. 2013). The WRF-Lake model is also able to reproduce the spatial pattern of T_{2m} (Fig. 3d–f) with a bias of –1.2 °C when averaged over the TP. It is presumed that the unrealistic description of topography contrast over the TP is also the main cause for the large negative bias in T_{2m} simulations especially over the steep Himalayas. Despite some regional biases, the evaluation results suggest that the WRF-Lake model can reasonably capture the general spatial patterns of summer precipitation and T_{2m} over the TP and surrounding areas.

To give a comprehensive evaluation of the model performances, we depict several important Taylor statistics based on the summer mean precipitation and T_{2m} over the two model domains in Fig. 14 and Table 1. From the Taylor diagram in Figure 14, it is evident that with the horizontal resolution increases, the model shows better capability in reproducing the spatial distribution of both precipitation and T_{2m}. In addition, as indicated by high PC, TS and low RMSE for the CTRL modeled summer precipitation and T_{2m} over the inner domain (D02) (Table 1), the WRF-Lake model is an appropriate tool to identify the climatic effect of the TP lakes in summer.

4 Climatic effect of the TP lakes

4.1 Lake Effects on the 2-m air temperature

The impacts of the TP lakes on T_{2m} at local to regional scales are quantified based on the differences between the simulations from the experiments with and without lakes over the TP (Figs. 4 and 5). From Fig. 4a, b, the T_{2m} differences with the statistical significance level of 0.05 (two-tailed t test) are mainly confined to the lake areas over the TP, indicating that the TP lakes mainly display local effects on T_{2m}. Hence, we further select a sub-region bounded by 30°N–36°N and 80°E–92°E (i.e. the red rectangle in Fig. 4b), which is also referred as central TP (CTP) covering most of TP lakes for more detailed analysis. From Fig. 4c, the mean terrain height of the CTP is above 4400 m and the topography is characterized by a middle low center and the surrounding high sides. As the major water sources for the lakes over this area are the glacial melt, the thawing permafrost, and the precipitation, most lakes were formed in the lowlands. The major large lakes, i.e. Lake Siling Co and Lake Nam Co, are situated in the relatively moist southeastern CTP (bounded by 30°N–33°N, 80°E–86°E) (Biermann et al. 2014; Liu et al. 2010). Comparing the lake locations (Fig. 4c) and the CTRL-NOL T_{2m} differences (Fig. 4d), it is clear that the lakes in the western and northeastern CTP (bounded by 30°N–36°N, 80°E–86°E, and 33°N–36°N, 86°E–92°E, respectively) exert a significant cooling effect on the over-lake near-surface air temperature with a mean intensity above 2 °C, while the lakes over the southeastern CTP tend to slightly increase the over-lake T_{2m} with a mean magnitude about 0.15 °C. The remarkable cooling effect of the lakes in the western and northeastern CTP hardly exceed the lake shores, which is different from the prominent downwind influence of the Lake Victoria and the Laurentian Great Lakes due to the much wider lake coverage and the flatter orography (Notaro et al. 2013; Thiery et al. 2015). From Fig. 4b, d, almost all of the TP lakes display a cooling effect on T_{2m} over the surrounding land areas, particularly for those around the large lakes (i.e. Qinghai Lake) or over the lake-abundant regions (i.e. the southeastern CTP).

Figure 5 further reveals the sub-seasonal and diurnal variations of the lake effects on the T_{2m}, sensible and latent heat fluxes averaged over all the pixels and the lake pixels in the sub-region indicated by Fig. 4b. For all the pixels in the sub-region, the presence of TP lakes tend to cool the T_{2m}, weaken the upward sensible heat flux and enhance the upward latent heat flux at daily time scale (Fig. 5a–c); this effect is much more obvious over the lake pixels (Fig. 5d–f). Overall, the lake effects on all of the

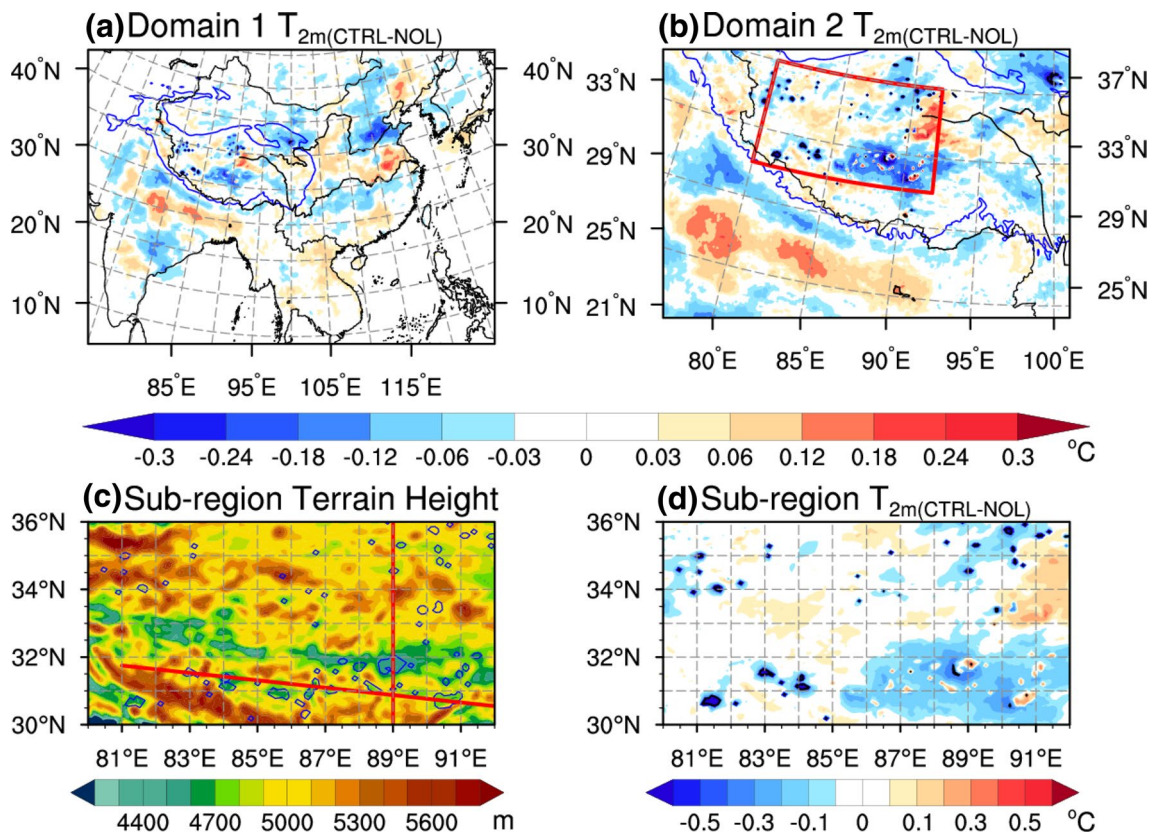


Fig. 4 The simulated summer mean T_{2m} differences between CTRL and NOL in **a** Domain 1, **b** Domain 2, and **d** the sub-region (30°N–36°N, 80°E–92°E) which is outlined by the red polygon in **b** averaged over 2008–2014. The thicker black curves (circles) in **a**, **b** and **d** represent the differences that are statistically significant at the 5% level (two-tailed t test). **c** The spatial distribution of TP lakes

(blue contours) and the terrain height (shadings) in the sub-region. In (**a**–**b**), the blue curves outline the TP, while the black curves depict the Yangtze River and the Yellow River. The red line in **c** represents the transections used for the vertical cross sections in Figs. 12 and Figure A2

above thermal variables are generally localized and only significant over the lake areas. The lakes induce a persistent over-lake cooling of about 1 °C throughout the entire summer (Fig. 5d). Meanwhile, the effects of TP lakes on the upward sensible (latent) heat flux show a pronounced decreasing (increasing) trend from early to late summer (Fig. 5e, f). At the diurnal time scale (Fig. 5j, g), the lakes exhibit a cooling (warming) effect on T_{2m} during daytime (nighttime) and therefore dampen the diurnal variations of T_{2m} ; this is particularly true when only consider the lake pixels in the sub-region (Fig. 5j). Meanwhile, the presence of the TP lakes can lead to decreases (increases) in the upward sensible and latent heat fluxes during daytime (nighttime) (Fig. 5h, i, k, l). As the lakes in the western and northeastern CTP are characterized by a dominant daytime cooling and slight nighttime warming (figure not shown), these lakes exhibit a general net cooling influence on the over-lake T_{2m} in summer (Fig. 4d). However, the strength of the nighttime warming due to the lakes in the southeastern CTP is relatively larger than the daytime

cooling (+1.75 °C vs. – 1.45 °C), leading to a slight net warming effect on the over-lake T_{2m} in summer (Fig. 4d).

Figures 6 give an overview of the lake-induced net changes in the main component of the surface heat balance equation (i.e. Eq. 5) and the relative contribution of each factor in Eq. 6 to δT_s over the lakes at daily time scales during summer. As the lake presence lowers the surface albedo and the daytime cloud coverage (figures not shown), the over-lake surface net shortwave radiation (SW_{net}) is increased by 53 Wm^{-2} (Fig. 6a). Meanwhile, the lakes strengthen the upward LHF by 63 Wm^{-2} and weaken the upward SHF by 46 Wm^{-2} over the lake surfaces. In addition, it is also noted that the lakes lead to an increase of 57 Wm^{-2} in heat storage (G) due to the much larger thermal inertia relative to the land surfaces. The decreased outgoing longwave radiation due to the cooler lake surface results in relatively larger net downward longwave radiation (LW_{net} , 21 Wm^{-2}) at the lake surfaces (Fig. 6a).

From Fig. 6b, the changes in the surface albedo, SW_{in} , upward SHF and surface emissivity [LW_{in} , upward LHF,

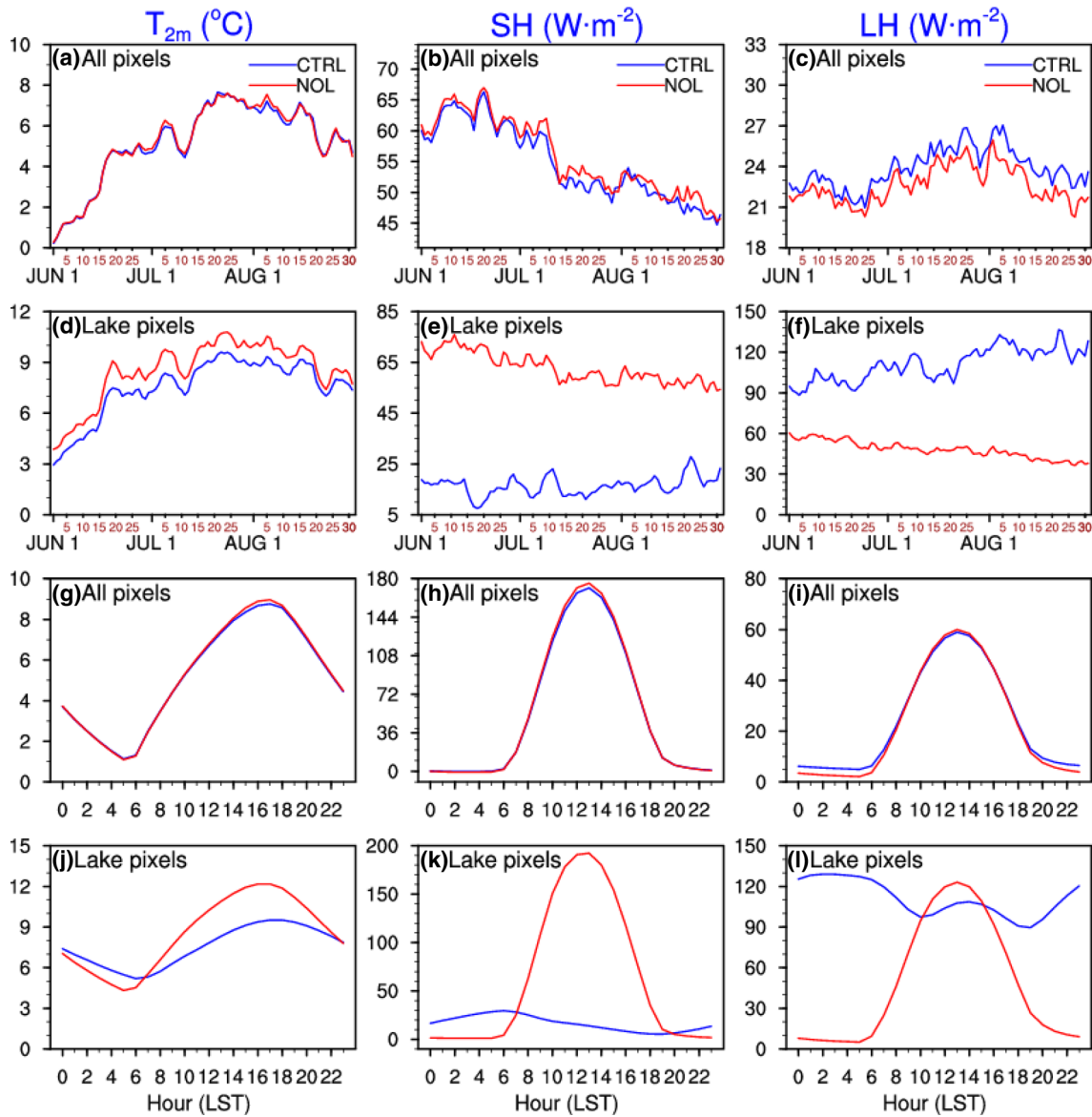


Fig. 5 The CTRL and NOL modeled sub-seasonal (a–f) and diurnal cycles (g–l) of the mean T_{2m} (left panel), sensible heat flux (middle panel) and latent heat flux (right pane) over 2008–2014 region-

ally averaged over the all pixels and lake pixels in the sub-region (30°N–36°N, 80°E–92°E)

subsurface heat flux (G) induced by the TP lakes tend to exert positive (negative) contribution to the over-lake δT_s . The lake-induced increase in the upward LHF contributes the most to δT_s by $-13.05\text{ }^\circ\text{C}$ over the lakes. The increased subsurface heat flux (G) due to the presence of lakes results in a cooling of the surface by $7.44\text{ }^\circ\text{C}$. Both the increased aerodynamic resistance due to the smaller roughness length of lake surface relative to the nearby land and the decreased temperature gradient in the atmospheric surface layer (Thiery et al. 2015) lead to the decreased upward SHF and therefore act to increase the T_s by $7.43\text{ }^\circ\text{C}$, presenting the largest warming effect on T_s . The increase in SW_{in} induced by the reduction of the daytime cloud cover over the lakes

contribute to the δT_s by $5.59\text{ }^\circ\text{C}$. The much lower albedo of the lake surface results in a positive contribution to $[\delta T_s]$ of $3.70\text{ }^\circ\text{C}$ over the lakes. Contributions of the changes in surface emissivity and in LW_{in} due to the cloud cover and atmospheric temperature changes are negligible. Eventually, the TP lakes lead to a cooling effect on both T_s ($-4.73\text{ }^\circ\text{C}$) and T_{2m} ($-0.97\text{ }^\circ\text{C}$) over all the lake pixels in the sub-region on average. Compared to the surrounding land, the enhanced evaporation from the lakes and larger heat inertia of water result in lower T_s and thereafter reduced temperature gradient between the lake surface and overlying atmosphere. The reduced temperature gradient and smaller roughness length of lake surface work together to dampen the SHF release

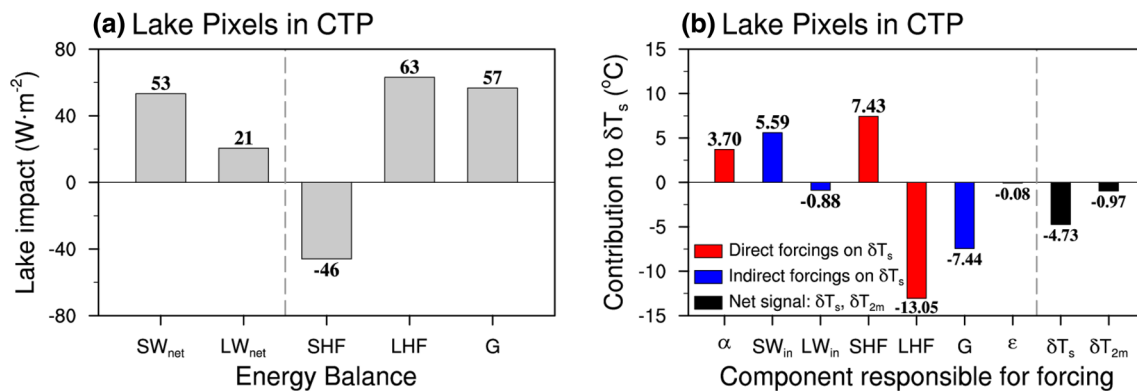


Fig. 6 **a** Lake-induced changes in the surface energy balance components SW_{net} , LW_{net} , SHF, LHF, and G (all units: $W\ m^{-2}$) averaged over the lake pixels in the sub-region ($30^{\circ}N$ – $36^{\circ}N$, $80^{\circ}E$ – $92^{\circ}E$). **b** Individual direct (red), indirect (blue) contributions of albedo α ,

SW_{in} , LW_{in} , SHF, LHF, and G to δT_s and the net δT_s and δT_{2m} signal (black) derived from the mean differences between CTRL and NOL simulations averaged over the lake pixels in the sub-region

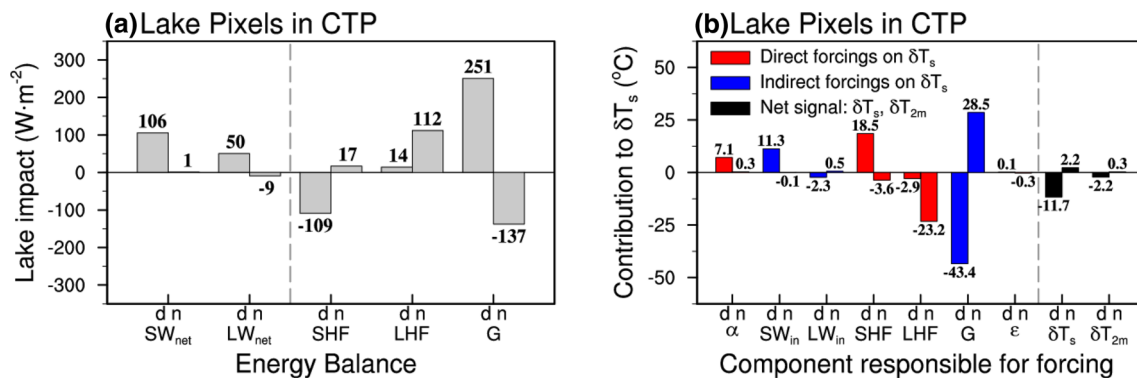


Fig. 7 Same as Fig. 7, but for now separately for 09:00–18:00 LST (daytime; shown as d) and 18:00–09:00 LST (nighttime; shown as n) for all the lake pixels in the sub-region ($30^{\circ}N$ – $36^{\circ}N$, $80^{\circ}E$ – $92^{\circ}E$)

from the lake surface to the atmosphere and further lead to the decreased T_{2m} over the lake areas.

To illustrate changes at sub-daily time scales, Fig. 7 further gives the changes in each surface heat balance component and the contribution of the seven factors to δT_s over lakes in the sub-region during daytime and nighttime. Comparing Fig. 7a with Fig. 6a, the decreases of the daily-mean upward SHF over the lake areas is dominated by the daytime inhibition, and the enhanced daily-mean LHF (SW_{net} and LW_{net}) is mainly attributed to the remarkable nighttime (daytime) increases. In contrast, the lake-induced changes of ground heat flux (G) display obvious diurnal variation, with more heat stored in the subsurface and deep waters during daytime ($251\ Wm^{-2}$) and more heat released from the lake mixed layer during nighttime ($137\ Wm^{-2}$, Fig. 7a). During daytime, the lake-induced changes in G exert a pronounced cooling effect on T_s and it is decreased by $11.7\ ^{\circ}C$ on average (Fig. 7b). Meanwhile, the decreased T_s and upward temperature gradient further inhibits the upward SHF and thus leads

to the reduced over-lake T_{2m} by $2.2\ ^{\circ}C$ (Figs. 5j and 7b). However, during nighttime the enhanced released G from the sub-surface and deep waters to the surface (Fig. 7a) leads to a warming of the lake surfaces and T_s is increased with a mean intensity of $2.2\ ^{\circ}C$ (Fig. 7b), which favors the SHF transfer from surface to the atmosphere with the intensity of $17\ Wm^{-2}$ (Fig. 7a) and leads to an increase of $0.3\ ^{\circ}C$ in the over-lake T_{2m} (Fig. 7b). In general, the daytime cooling dominates the daily-mean changes for both δT_s and δT_{2m} over the lake (Figs. 6b and 7b).

4.2 Lake effects on the precipitation

The CTRL-NOL differences in the total rainfall (TR), convective rainfall (CR), and large-scale rainfall (LSR) over the domain 1, domain 2, and the sub-region indicated by Fig. 4b are shown in Fig. 8. In contrast to the very localized influences of the TP lakes on the T_{2m} , the lake effects on precipitation, especially CR, can extend to the lake

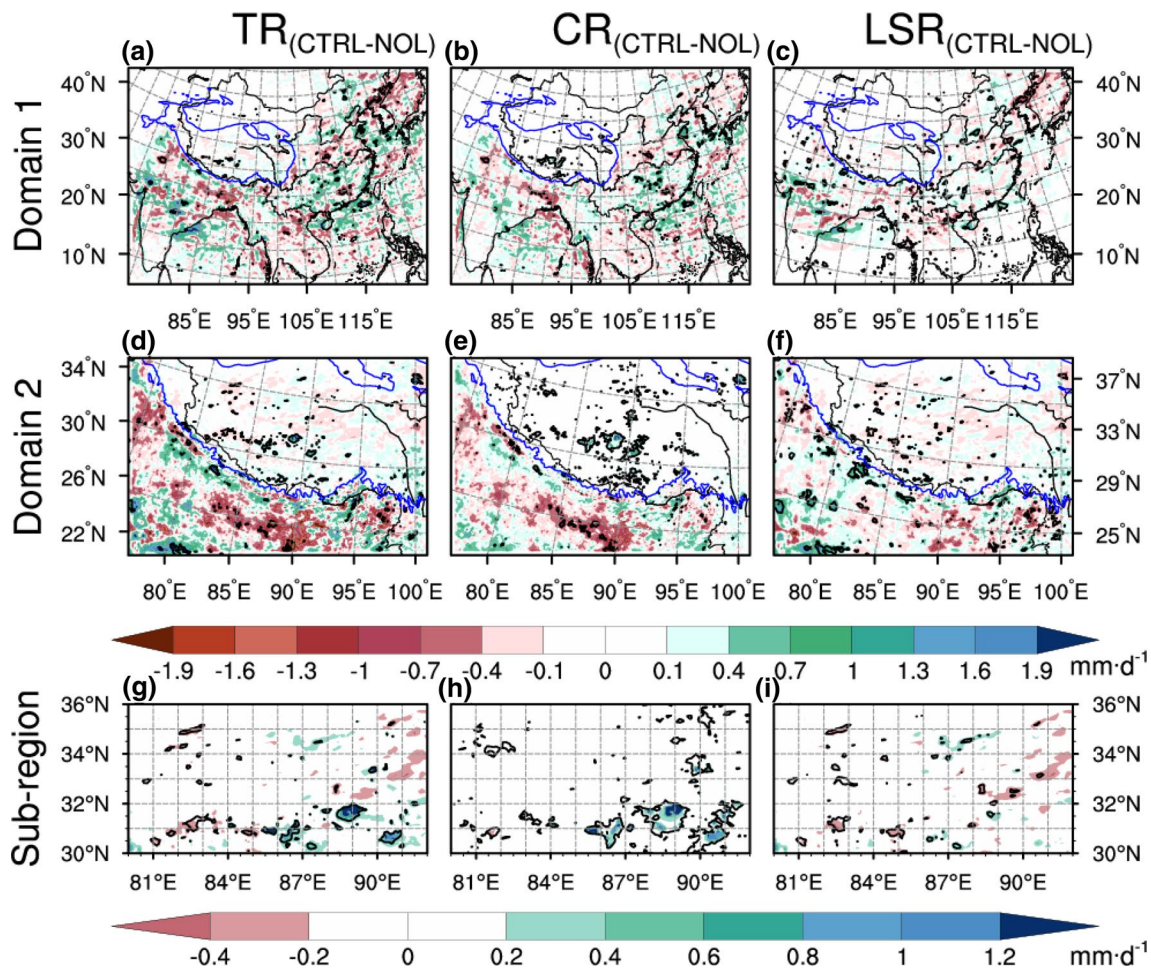


Fig. 8 The simulated summer mean total rainfall (TR, left panel), convective rainfall (CR, middle panel), and large-scale rainfall (LSR, right panel) differences between CTRL and NOL averaged over 2008–2014 in the Domain 1, Domain 2, and the sub-region (30°N–36°N, 80°E–92°E) which is outlined by the red polygon in

Fig. 5b. The thicker black curves in a–i represent the differences are statistically significant at the 5% level (two-tailed t test). In a–f, the blue curves outline the TP, while the black lines depict the Yangtze River and the Yellow River

surrounding areas although the precipitation changes are not as significant as that over the lake regions (Fig. 8a–f). As shown in Fig. 8g, the lakes in the southeastern CTP tend to enhance the TR by 0.95 mm day^{-1} with the relative change of 36%. However, the other lakes in CTP mainly exhibit inhibition impacts on TR and the overall influence on TR is a slight increase with a magnitude of $0.043 \text{ mm day}^{-1}$ (relative change of +3.6%). This slightly increased TR averaged over the lakes in the western and northeastern CTP can be attributed to the relatively larger CR enhancement over several lakes centered at (31.3°N, 84°E), (30.8°N, 86°E), and (33.2°N, 89.9°E) compared to the decrease of CR and LSR over the other lakes in the western and northeastern CTP. While, the increased TR over the lakes in the southeastern CTP is mainly attributed to the CR enhancement (Fig. 8g, h). These disparate lake effects on the precipitation will be further investigated in Sect. 4.3.

At sub-seasonal and diurnal scales, the lake-induced LSR responses are negligible when averaged over the lake pixels in the sub-region (Fig. 9f, i), but the lake can induce evident increases in the TR and CR, particularly during the post-monsoon period (Fig. 9d, e) and nighttime (Fig. 9j, k). The enhanced moisture and energy releases play important roles in triggering the local convective precipitation in the post-monsoon period (figures not shown). The TR averaged over the CTP displays two diurnal peaks at mid-night and late-afternoon, with the former one associated with the LSR peak and the latter one with the CR peak (Fig. 9g–i). However, the TR averaged over the lake areas in CTP only presents a single strong diurnal peak from mid-night to early morning and the minimal TR occurs at around 14:00 LST (Fig. 9j). From Figs. 5j–l and 9j–l, it can be speculated that due to the large thermal inertia and the low surface roughness, the TP lakes tend to largely weaken (strengthen) the upward

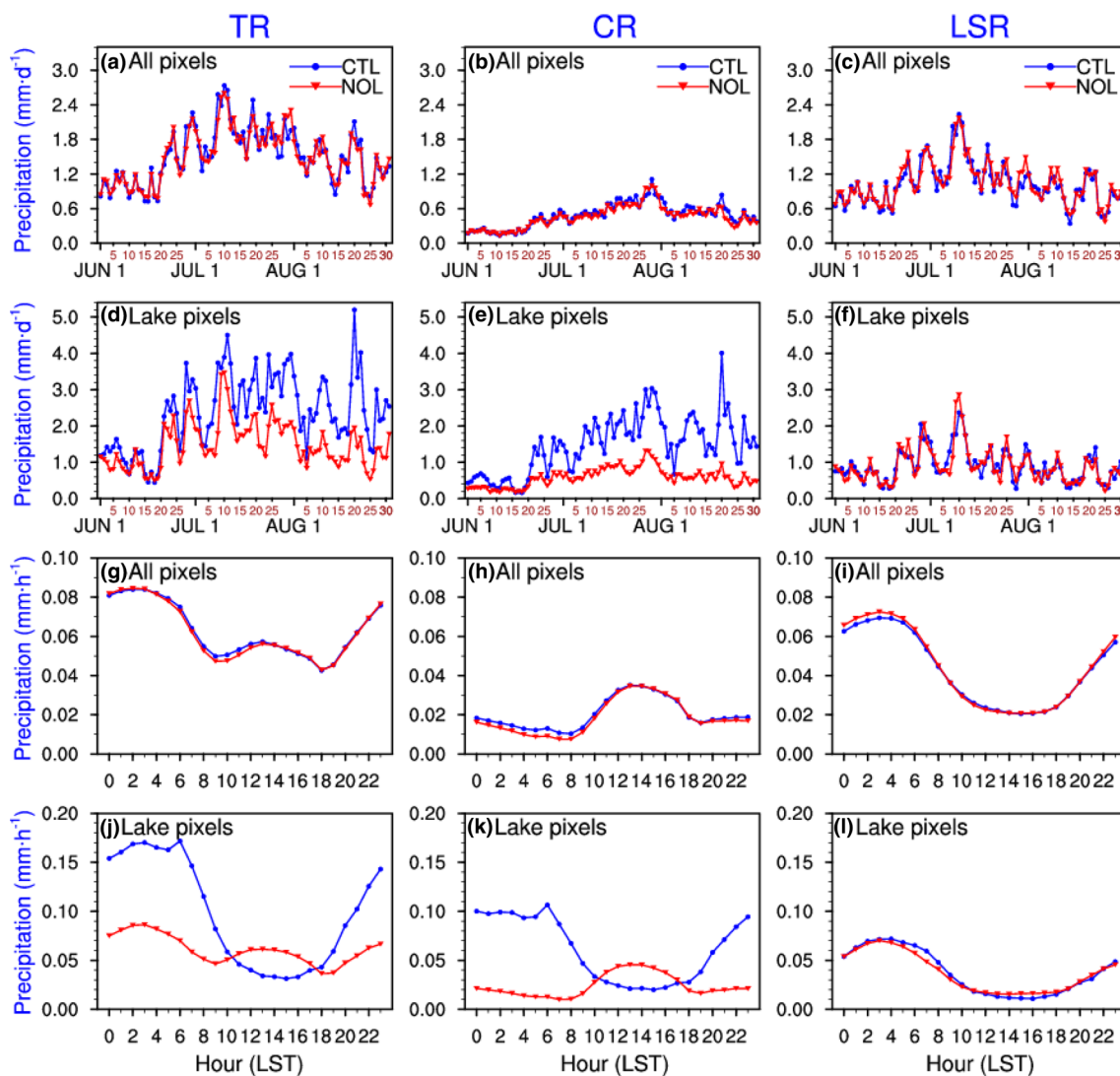


Fig. 9 The CTRL and NOL modeled sub-seasonal (a–f) and diurnal cycles (g–l) of the mean total rainfall (TR, left panel), convective rainfall (CR, middle panel), and large-scale rainfall (LSR, right panel)

over 2008–2014 regionally averaged over the all pixels and lake pixels in the sub-region (30°N–36°N, 80°E–92°E)

SH, cool (warm) the near-surface air temperature, stabilize (destabilize) the over-lake atmosphere, and therefore inhibit (enhance) the CR and TR during daytime (nighttime). In specific, the lakes in the southeastern CTP lead to decreases of 0.09 mm day^{-1} (relative change of 28%) in the daytime TR and increases of 1.04 mm day^{-1} (relative change of 45%) in the nighttime TR, respectively. The lakes in the western and northeastern CTP tend to decrease the daytime TR by 0.05 mm day^{-1} (relative change of -16%) and enhance the nighttime TR by 0.10 mm day^{-1} (relative change of $+11\%$).

Figures 10 and 11 further give a detailed discussion on the lake-induced changes of precipitation with different duration times. According to the previous studies, mesoscale convective systems are prevalent over the CTP during summer and the rainfall is characterized by small amount, high

frequency, and weak intensity (Feng et al. 2014; Fu et al. 2006; Gao et al. 2016). In this study, the CTRL experiment well reproduces such rainfall features with the averaged PA less than 0.06 mm h^{-1} , the maximal PF exceeding 48%, and the mean PI at 0.64 mm h^{-1} over the sub-region (figures not shown), which gives us some confidence to use the model outputs to investigate the lake effects on PA, PF, and PI over the CTP. From Fig. 10a–c, the lakes in the southeastern CTP induce a strong enhancement on the total rainfall PA by concurrently increasing both the short-duration and long-duration PA, while the simulated total rainfall PA in the western and northeastern CTP shows slightly significant changes. For the total and short-duration rainfall, the increase in the PA (Fig. 10a, b) over the southeastern CTP is mainly contributed by the enhanced PI (Fig. 10g, h), although the

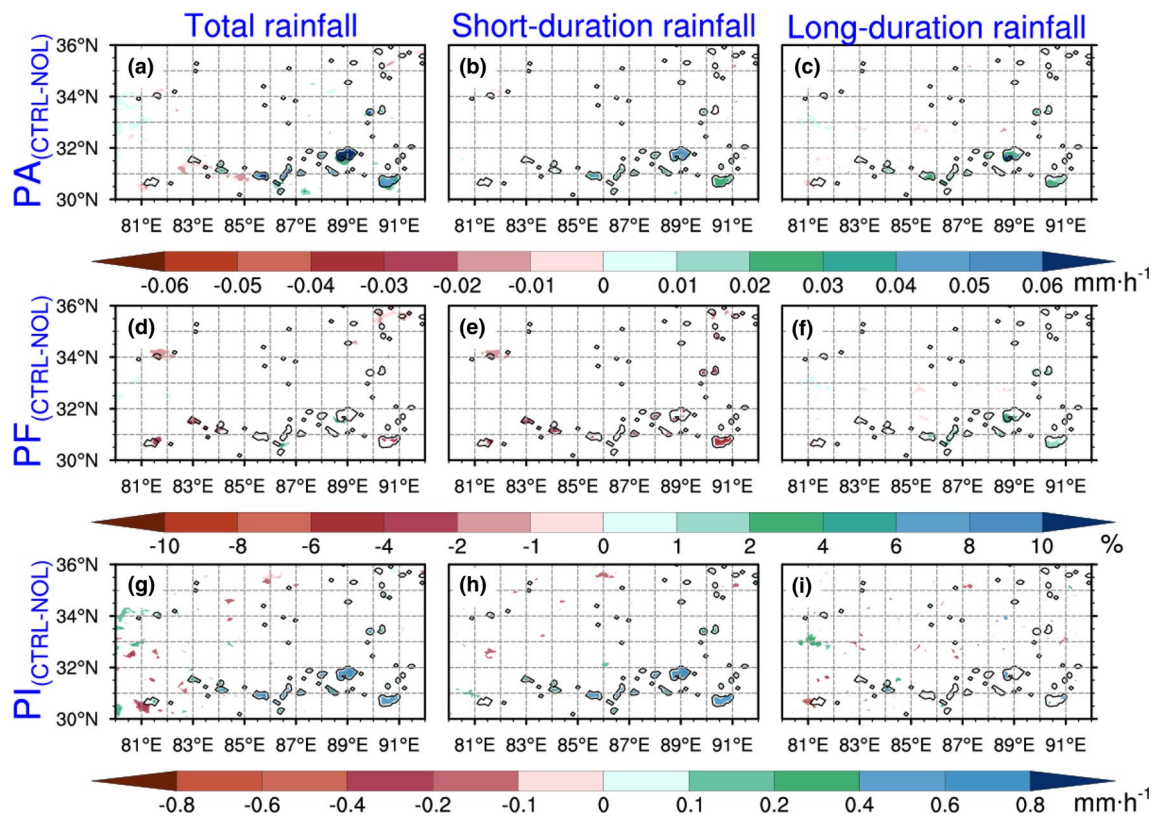


Fig. 10 The differences of the simulated PA, PF and PI for the total (left panel), short-duration (middle panel), and long-duration (right panel) rainfall between CTRL and NOL in the sub-region averaged

over 2008–2014. The shadings in **a–i** represent the differences are statistically significant at the 5% level (two-tailed *t* test). The black curves outline the locations and ranges of TP lakes

PF is weakened due to the presence of lakes (Fig. 10d, e). However, the lakes in the southeastern CTP tend to increase both the PF and PI (Fig. 10f, i) and thereafter PA for the long-duration rainfall (Fig. 10c).

From Fig. 11, the PA, PF and PI for the total and short-duration rainfall display analogous diurnal cycles regardless of their different magnitudes. Specifically, the lakes in the CTP can enhance the PI of the over-lake total and short-duration rainfall throughout the entire day due to the persistent upward water vapor transport (Fig. 11g, h). The original nighttime PA peaks of the total and short-duration rainfall are enhanced by the lake-induced increases in PI and PF during late evening to early morning, while the late-afternoon peak of PA is slightly weakened by the sharply decreased PF during 12:00–18:00 LST (Fig. 11a, b, d, e). For the long-duration rainfall, the TP lakes show an enhancement effect on all of the PA, PF, and PI during late evening to early morning (Fig. 11c, f, i).

In general, the effects of the TP lakes, primarily the lakes in the southeastern CTP, on precipitation occur both on the lake and the surrounding areas, which can be referred as the downwind phenomenon of lake effect precipitation (Dai et al. 2018; Notaro et al. 2013; Wen et al. 2015b). Owing

to the small surface roughness length and large water vapor supply of the lakes, the background southwest wind can be accelerated and moistened when passing the lakes in the southeastern CTP (figures not shown). The accelerated humid air mass would further converge and arise over the lake and the downwind regions and promote more convective development over there. At the diurnal time scale, the TP lakes can strengthen the CR during late evening to early morning and weaken the CR during afternoon (12:00–18:00 LST). The influence of the TP lakes on the CR gradually intensifies after the onset of the summer monsoon and culminates in the post-monsoon period, leading to an increase of 3.06 mm day^{-1} in CR (relative change of 76%). Moreover, it is noteworthy that all the TP lakes can suppress the daytime CR whereas only the lakes in the southeastern CTP exert a significant enhancement effects on the nighttime CR. These disparate features further suggest that the effects of the TP lakes on the precipitation are not only affected by the background atmospheric circulations (Ruthrich et al. 2015), but also largely influenced by the lake natures and surrounding topography contrast. In terms of the precipitation duration time, the inhibition effect of the TP lakes on daytime rainfall is ascribed to the large decrease of afternoon

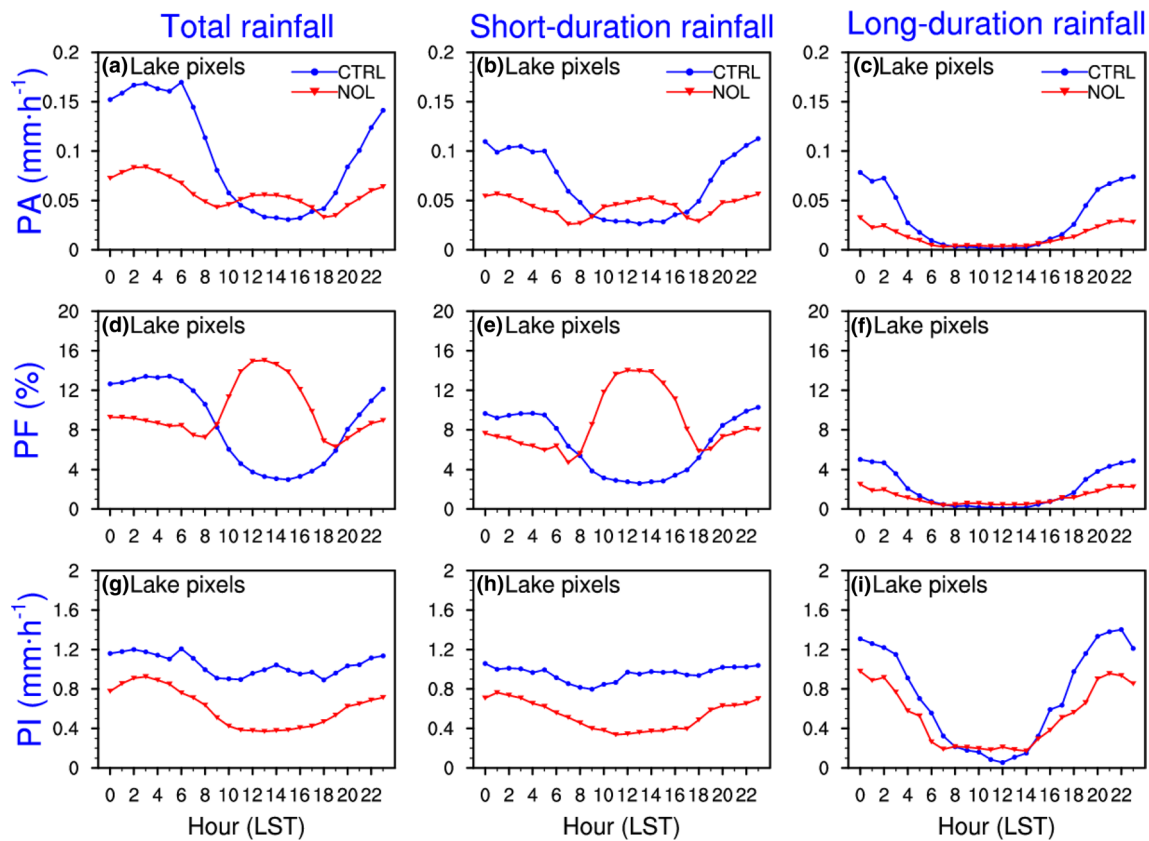


Fig. 11 The modeled diurnal cycles of the mean PA, PF, and PI for the total rainfall (left panel), short-duration rainfall (middle panel), and long-duration rainfall (right panel) over 2008–2014 regionally averaged over the lake pixels in the sub-region (30°N–36°N, 80°E–92°E)

short-duration PF and PA. The lake-induced enhancement in the nighttime rainfall over the southeastern CTP is attributed to the simultaneous increases in the PA, PF and PI for the short-duration and long-duration rainfall during late evening to early morning.

4.2.1 Dynamical response to the presence of the TP lakes

Following Thiery et al. (2015), we employ two vertical transections indicated by the solid red lines in Fig. 4c, one of which crosses the Lake Siling Co and a northern smaller lake (Lake Dogai Coring centered at 34.5°N, 89°E), to investigate the disparate atmospheric response to the lakes with different sizes and locations. Based on the diurnal variations of the TP lakes' influence on T_{2m} and precipitation (Figs. 5 and 9), we select 12:00–18:00 LST and 02:00–08:00 LST as two typical periods in a day for understanding the lakes' cooling/precipitation inhibition effects and warming/precipitation enhancement effects, respectively. Then, we carried out the daytime and nighttime composites of the differences between the

CTRL and NOL experiments averaged over the above typical periods in a day during 2008–2014 (Fig. 12).

During the daytime, the TP lakes cool and moisten the overlying atmosphere (Fig. 12a, c). According to Eq. 7, the abundant water vapor fluxes injecting into the boundary layer tend to increase the low-level θ_e and therefore destabilize the atmospheric column over Lake Siling Co. However, the enhancement of the θ_e is confined below ~ 5.2 km due to the strong daytime cooling effect of lake that suppresses the boundary layer mixing (Fig. 12a, c, e). From Fig. 12e, the upper θ_e increases and extends up to ~ 8 km, indicating a stable over-lake boundary layer. Meanwhile, as most larger lakes are situated in lowlands (Fig. 4c), the surrounding hillsides with lower heat capability can receive more solar radiation, warm up faster, and therefore lead to the over-land ascending motions and the lake breeze due to the lake-land thermal contrast (Biermann et al. 2014; Gerken et al. 2013). On one hand, such secondary circulation with prevalent subsidence wind and divergent flow above lake are not favorable for the development of over-lake convection during daytime. On the other hand, as the over-lake moist air is advected by the lake breeze and further rises up slope following

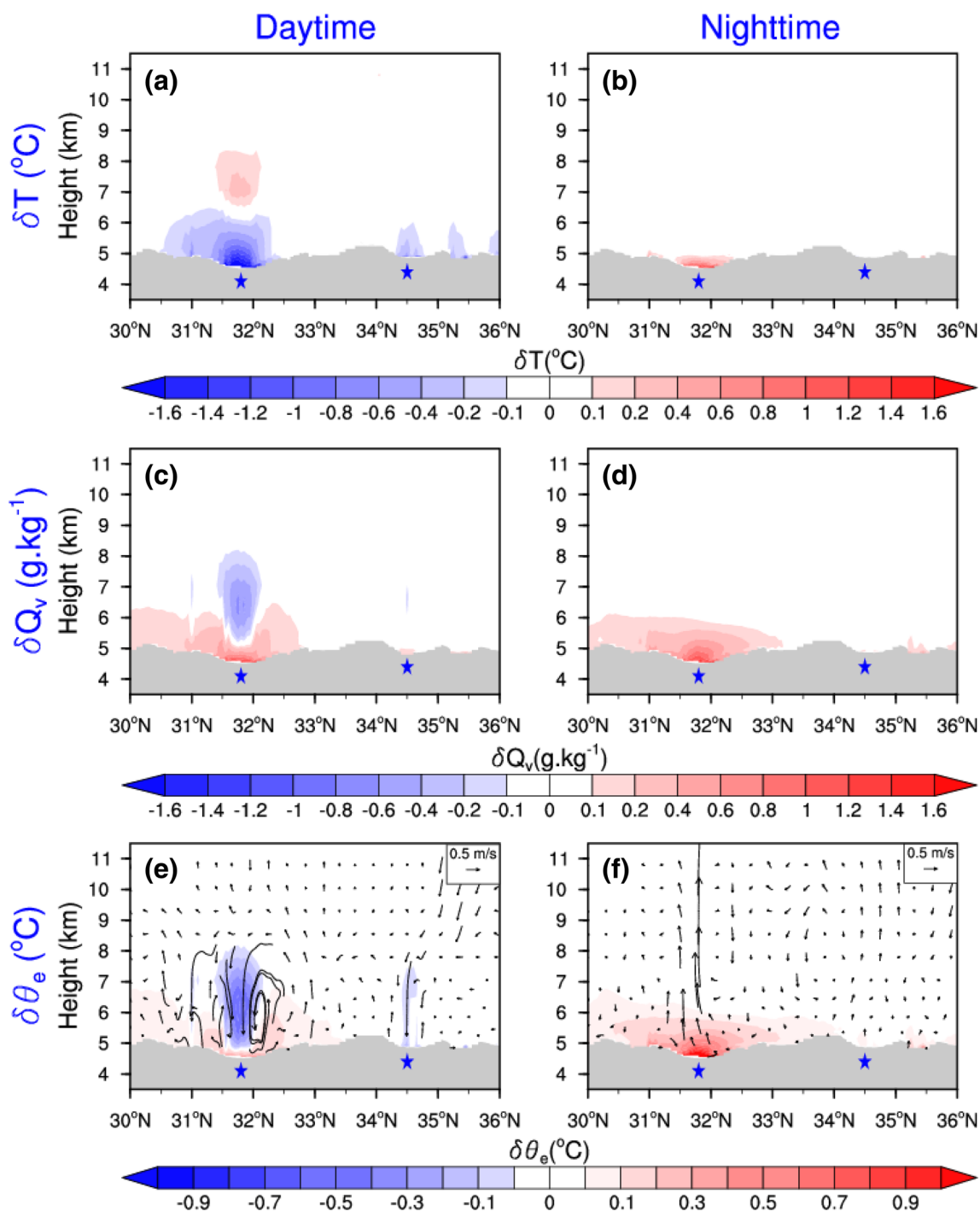


Fig. 12 The height-latitude cross sections along 89°E of the simulated mean differences in the T_{2m} (top), specific humidity (middle), and equivalent potential temperature (shaded) with the longitudinal circulation (vectors, units: $m s^{-1}$) (bottom) during the daytime (12:00–18:00 LST) and nighttime (02:00–08:00 LST) over 2008–

2014. The vertical velocity was enlarged by 100 times. The gray shaded areas denote the terrain height. The sunken areas marked by blue stars around the 32°N and 34.5°N roughly represent the locations of Lake Siling Co and Lake Dogai Coring, respectively

the anabatic wind, the over-land atmosphere is destabilized and favorable for the development of CR shown in Fig. 8h. While, this daytime unstable signal over land is relatively weaker and dissipates more quickly compared

to the nighttime one over lake areas (Fig. 12f), which may explain why the lake-induced CR enhancement over lake areas is stronger than that in the surrounding regions (Fig. 8h).

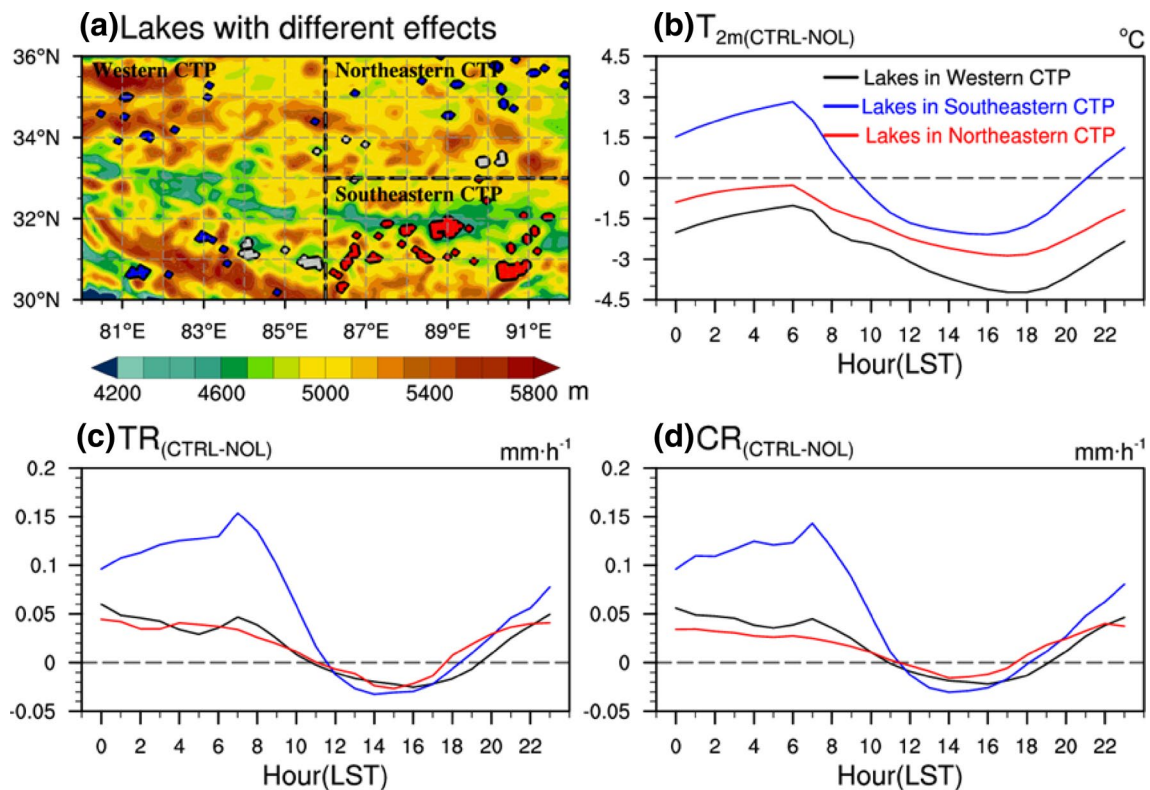


Fig. 13 Spatial distributions of the lakes with persistent cooling and precipitation inhibition effects (shaded in blue), the lakes with a general cooling effect and slight precipitation enhancement effects (shaded in gray), and the lakes with a general warming and strong precipitation enhancement effects (shaded in red) over the sub-region (30°N – 36°N , 80°E – 92°E). The diurnal cycles of the modeled

T_{2m} (b), TR (c) and CR (d) differences between CTRL and NOL regionally averaged over the southwestern (black lines, 30°N – 33°N , 80°E – 86°E), the southeastern (30°N – 33°N , 86°E – 92°E), and the northern (33°N – 36°N , 80°E – 92°E) CTP indicated in (a). The shadings in a denote the terrain height

At nighttime, accompanied by the plenty release of the upward latent heat from the lake surface, the over-lake atmosphere is warmed and moistened (Fig. 12b, d). In contrast to the canceling effect of lower air temperature and higher specific humidity on the atmospheric stability during daytime, the nighttime warming and moistening effect reinforce each other in generating the unstable boundary layer up to ~ 6 km over the Lake Siling Co (Fig. 12f), resembling the African Great Lakes' effect (Thiery et al. 2015; Verburg and Antenucci 2010). Driven by the opposite lake-land thermal contrast, the secondary circulation is effectively reversed during nighttime, featuring strong over-lake ascending motions and a land breeze (Fig. 12f). At the same time, the nighttime downhill wind can not only enhance the over-lake convergent

flow and the anabatic winds, but also advect abundant cold dry air, which is further warmed and moistened by the relatively warmer and wetter water surface and results in the increase of over-lake CR (Fig. 8h). Different from the large lakes, the small lake in the northeastern CTP acts to cool the overlying air and stabilize the atmospheric column during daytime (Fig. 12a, c and e), but has rather small impacts on the LH release and the over-lake air properties during nighttime (Fig. 12b, d and f). From Fig. 15a, c and e, it can be also seen that during daytime, there exist prevalent divergent katabatic winds above all of the lakes along the east–west cross section due to the strong lake-induced cooling effects, which is unfavorable for the over-lake CR development. However, the lake-induced warming and moistening effects during nighttime

can only be detected around the lakes areas in southeastern CTP and two small lakes (centered at 31.2°N, 83.5°E in Fig. 4c) over the western CTP (Fig. 15b, d and f). The different climatic effects of the above two lakes and another nearby lake with a similar lake size centered at (31.5°N, 83°E) further emphasize that the mountain-valley system triggered by the local orographic contrast exerts important additive effects on the lake influences.

As the above two cross sections only pass several lakes over CTP, we further give the spatial distributions of lakes with different climatic effects over CTP and obtain the overall influences of the lakes over southeastern, western, and northeastern CTP on T_{2m} and precipitation. Based on the different lake influences on T_{2m} and precipitation, the lakes over the CTP are classified into three categories: (1) lakes acting to cool the near-surface air and suppress the precipitation throughout the whole day; (2) lakes with a general cooling effect (stronger daytime cooling vs weaker nighttime warming) and a slight precipitation enhancement effect during nighttime; and (3) lakes with a general warming effect (weaker daytime cooling vs stronger nighttime warming) and a strong precipitation enhancement effect during nighttime. As seen in Fig. 13, most lakes in the western and northeastern CTP tend to cool the over-lake air and stabilize the boundary layer throughout the whole day and the mean over-lake precipitation during nighttime is slightly enhanced due to the CR enhancement over several lakes (shaded gray in Fig. 13a). Contrastingly, the lakes in the southeastern CTP all act to show strong heating and destabilization effects on the over-lake air and therefore largely enhance the CR during nighttime. In general, the absence (presence) of nighttime warming and moistening effect of the lakes in the western and northeastern (southeastern) CTP is the main reason responsible for the overall cooling (warming) and precipitation inhibition (enhancement) pattern during summer.

5 Summary and discussion

In this study, we have investigated the climatic effects of the lake clusters over the TP in summer by applying a high-resolution air-lake coupled climate model WRF-Lake. Two 7-year (2008–2014) numerical simulations with and without the lakes in the TP were conducted to quantify to what extent the TP lakes can influence the climate at local to regional scales in summer.

We firstly evaluate the model's capability in simulating the LSWT, 2-m air temperature, and precipitation over the

TP and surrounding regions during summer. The results demonstrate that the CTRL experiment including the TP lakes can reasonably reproduce the daily variations of LSWT during summer, with a TC of 0.98 and a bias of approximately -0.4 °C for the LSWT simulations of Qinghai Lake when compared against the observations. Moreover, the WRF-Lake model shows good ability in simulating the T_{2m} and precipitation over the TP in terms of both magnitude and spatial pattern.

The TP lakes display obvious localized impacts on the T_{2m} , SH, and LH with the significant changes confined to the lake areas. Generally, the lakes tend to decrease the T_{2m} during summer and dampen the diurnal variability of T_{2m} due to the decrease (increase) of upward SH and T_{2m} during daytime (nighttime). Decomposition analysis indicates, that the lake-induced T_s changes are mainly attributed to the large subsurface heat storage in the lake, which acts to decrease (increase) the T_s and the temperature gradient between lake surface and overlying atmosphere, and thereafter decrease (increase) SHF and T_{2m} during daytime (nighttime). The magnitudes of the daytime cooling and nighttime warming effects vary with the lake locations. Specifically, the lakes in the western and northeastern CTP significantly reduce the T_{2m} by more than 2 °C, while the lakes in the southeastern CTP slightly increase the T_{2m} by 0.15 °C.

In contrast to the localized impact on the over-lake T_{2m} , the lake effects on the TR and CR can propagate to the surrounding areas forced by the lake and topography triggered circulations. The general lake effects on the precipitation also exhibits distinctive diurnal and sub-seasonal features: the TP lakes tend to reduce the short-duration PF and thereafter TR/CR during daytime, whereas increase the nighttime TR/CR via concurrently increasing the short-duration and long-duration PA, PF and PI. The lake-induced CR enhancement is generally stronger in the post-monsoon period than in early summer, indicating that the background atmospheric circulation may exert a superimposed effect on the lake and orographic influences. In terms of the lake locations, the lakes in the southeastern CTP tend to suppress the daytime rainfall but enhance the nighttime rainfall, while most lakes in the western and northeastern CTP only manifest to suppress the daytime precipitation.

Finally, a detailed composite analysis of the daytime and nighttime vertical transections crossing the Lake Siling Co and the Lake Dogai Coring is conducted to reveal the distinctive atmospheric responses to the presence of lakes with different lake sizes and during different times of day. During daytime, both the two lakes tend to decrease the low-level

air temperature, increase the surface air pressure, and trigger the over-lake divergent katabatic flow and lake breeze. Meanwhile, the valley wind can further enhance the above secondary circulation and suppress the over-lake convection during daytime. At nighttime, only the Lake Siling Co tends to increase the air temperature, moisten the over-lake air and result in the land breeze due to the positive lake-land thermal contrast. The lake-induced destabilization can be enhanced by the nighttime downhill wind in generating the convergent anabatic flow and more convective precipitation over the lake. The Lake Dogai Coring also tends to stabilize the boundary layer and suppress the precipitation during daytime, while it can hardly induce the over-lake convergent ascending motions and affect the precipitation during nighttime. Analogous results can be derived from the west–east-orientated transections, which explains why the lakes in the southeastern CTP exerts slight warming and remarkable precipitation enhancement effects, while most lakes in the western and northeastern CTP show general cooling and precipitation inhibition effects.

At present, the current lake model is a freshwater model and some key parameters (i.e. extinction coefficient, mixing factors) were calibrated by Gu et al. (2015) based on a set of studies on two plain lakes (Lake Erie and Lake Superior). Because most of the TP lakes located in the alpine cold climate zone are usually saline and rarely affected by the anthropogenic activities, the default lake model configurations could be inadequate to represent the distinctive characteristics of the lake internal thermal properties and lake-air interactions in the TP. In addition, the three-dimensional hydrodynamics, which is missing in the present lake model, may play important roles in the momentum balance, the heat redistribution, and therefore the LSWT simulations (Xue et al. 2016). Hence, to better understand the climatic effect of the TP lakes, future studies can utilize the 3-dimensional lake model with the empirical lake parameters calibrated particularly for the TP lakes. Additionally, present studies demonstrate that the lake intrinsic features, the local orographic contrast, and the background atmospheric circulations all exert significant impacts on the climatic effects of TP lakes, while it is hard to distinguish their individual contributions to the lake influences. However, it is anticipated that the use of finer-resolution climate simulations with improved lake schemes could be capable of providing more detailed descriptions and larger effective sample sizes of lake-air interactions for identifying the respective contributions of lake sizes, local orographic contrast, and background atmospheric circulations on the climate effects of lake clusters over TP during summer.

Acknowledgements This study is supported by National Key R&D Program of China under Grant2017YFA0604301, the National Natural Science Foundation of China under Grant91537102, Opening Fund of Key Laboratory of Land Surface Process and Climate Change in Cold and Arid Regions, Chinese Academy of Sciences (LPCC2016002), the Jiangsu University “Blue Project” outstanding young teachers training object, the Fundamental Research Funds for the Central Universities and the Jiangsu Collaborative Innovation Center for Climate Change. We thank Dr. Junbo Wang for providing us the bathymetry data of Lake Nam Co.

Open Access This article is distributed under the terms of the Creative Commons Attribution 4.0 International License (<http://creativecommons.org/licenses/by/4.0/>), which permits unrestricted use, distribution, and reproduction in any medium, provided you give appropriate credit to the original author(s) and the source, provide a link to the Creative Commons license, and indicate if changes were made.

Appendix A

Two additional figures are further given in this Appendix as follows: (1) Taylor diagram that depicts the pattern statistics between the CTRL simulations and observations for the summer precipitation and 2 m air temperature averaged over 2008–2014 (Fig. 14) and (2) same as Fig. 12, but for the vertical height-latitude cross sections along the west–east transection indicated by a red line in Fig. 4 (Fig. 15).

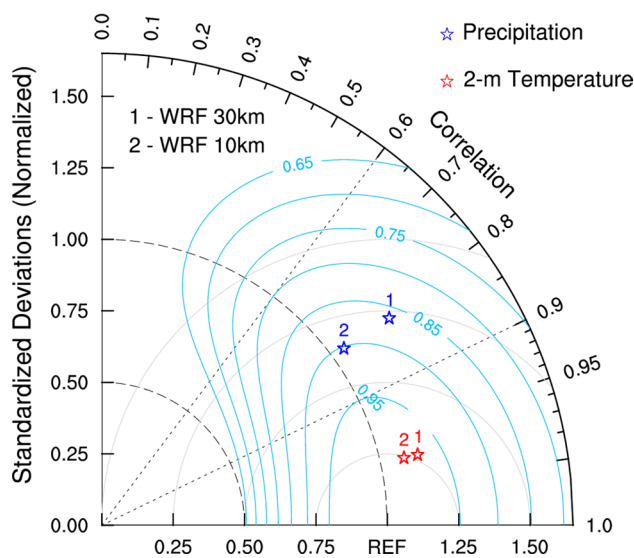


Fig. 14 Taylor diagram that depicts the pattern statistics between the CTRL simulations and observations for the summer precipitation (blue stars) and 2 m air temperature (red stars) averaged over 2008–2014. The radial distance from the origin represents σ . The cosine values of the angle of the star points from the horizontal axis give PC. The distance from the REF point indicates the normalized centered RMSE. The deep sky blue line with an interval of 0.05 represents the TS

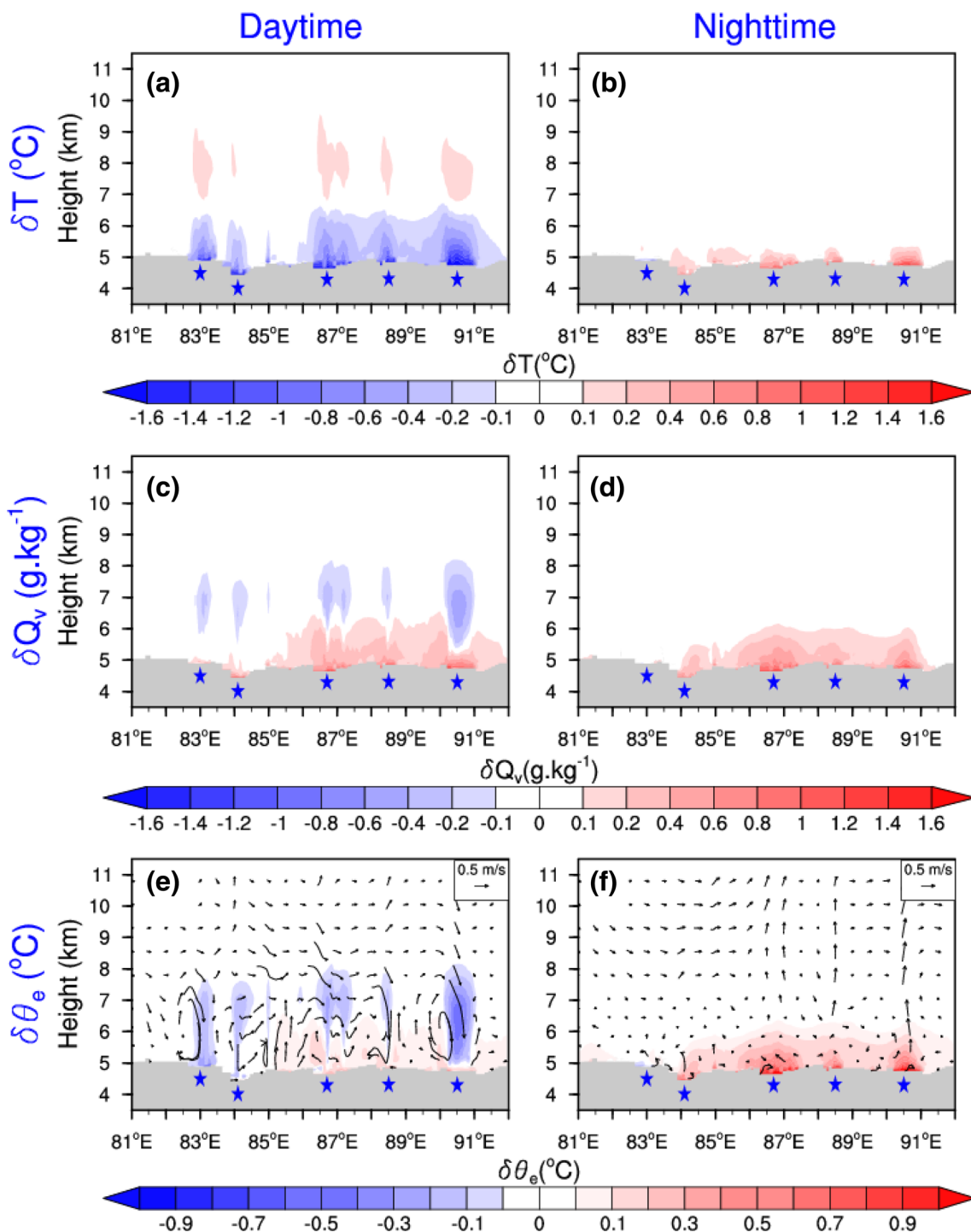


Fig. 15 Same as Fig. 12, but for the vertical height-latitude cross sections along the west–east transection indicated by a red line in Fig. 4

References

Adrian R, OReilly CM, Zagarese H, Baines SB, Hessen DO, Keller W, Livingstone DM, Sommaruga R, Straile D, Donk EV, Weyhenmeyer DA, Winder M (2009) Lakes as sentinels of climate change. *Limnol Oceanogr* 54(6part2):2283–2297. https://doi.org/10.4319/lo.2009.54.6_part_2.2283

Alcott TI, Steenburgh WJ, Laird NF (2012) Great salt lake-effect precipitation: observed frequency, characteristics, and associated environmental factors. *Weather Forecast* 27(4):954–971. <https://doi.org/10.1175/WAF-D-12-00016.1>
 Argent R, Sun X, Semazzi F, Xie L, Liu B (2015) The development of a customization framework for the WRF model over the Lake

- Victoria Basin, Eastern Africa on Seasonal Timescales. *Adv Meteorol* 4:1–15. <https://doi.org/10.1155/2015/653473>
- Bartunkova K, Sokol Z, Pop L (2014) Simulations of the influence of lake area on local temperature with the COSMO NWP model. *Atmos Res* 147:51–67. <https://doi.org/10.1016/j.atmosres.2014.05.003>
- Biermann T, Babel W, Ma W, Chen X, Thiem E, Ma Y, Foken T (2014) Turbulent flux observations and modelling over a shallow lake and a wet grassland in the Nam Co basin, Tibetan Plateau. *Theor Appl Climatol* 116:301–316. <https://doi.org/10.1007/s00704-013-0953-6>
- Bonan GB (1995) Sensitivity of a GCM simulation to inclusion of inland water surfaces. *J Chem Ecol* 8(11):2691–2704. [https://doi.org/10.1175/1520-0442\(1995\)008%3c2691:SOAGST%3e2.0.CO;2](https://doi.org/10.1175/1520-0442(1995)008%3c2691:SOAGST%3e2.0.CO;2)
- Choulga M, Kourzeneva E, Akharova E, Doganovsky A (2014) Estimation of the mean depth of boreal lakes for use in numerical weather prediction and climate modelling. *Tellus A*. <https://doi.org/10.3402/tellusa.v66.21295>
- Curtarelli MP, Alcántara EH, Rennó CD, Stech JL (2014) Physical changes within a large tropical hydroelectric reservoir induced by wintertime cold front activity. *Hydrol Earth Syst Sci* 18(8):3079–3093
- Dai Y, Wang L, Yao TD, Li XY, Zhu LJ, Zhang XW (2018) Observed and simulated lake effect precipitation over the Tibetan Plateau: an initial study at nam co lake. *J Geophys Res Atmos* 123:6746–6759. <https://doi.org/10.1029/2018JD028330>
- Davies HC, Turner RE (1977) Updating prediction models by dynamical relaxation: an examination of the technique. *Q J R Meteor Soc* 103:225–245. <https://doi.org/10.1002/qj.49710343602>
- Dudhia J (1989) Numerical study of convection observed during the winter monsoon experiment using a mesoscale two-dimensional model. *J Atmos Sci* 46:3077–3107. [https://doi.org/10.1175/1520-0469\(1989\)046%3c3077:NSOCOD%3e2.0.CO;2](https://doi.org/10.1175/1520-0469(1989)046%3c3077:NSOCOD%3e2.0.CO;2)
- Dutra E, Stepanenko VM, Balsamo G, Viterbo P, Miranda PMA, Mironov D, Schär C (2010) An offline study of the impact of lakes on the performance of the ECMWF surface scheme. *Boreal Environ Res* 15:100–112
- Feng XY, Liu CH, Rasmussen R, Fan GZ (2014) A 10-yr climatology of Tibetan Plateau vortices with NCEP climate forecast system reanalysis. *J Appl Meteor Climatol* 53:34–46. <https://doi.org/10.1175/JAMC-D-13-014.1>
- Friedl MA, Sulla-Menashe D, Tan B, Schneider A, Ramankutty N, Sibley A, Huang XL (2010) MODIS collection 5 global land cover: algorithm refinements and characterization of new datasets. *Remote Sens Environ* 114:168–182. <https://doi.org/10.1016/j.rse.2009.08.016>
- Fu YF, Liu GS, Wu GX, Yu RC, Xu YP, Wang Y, Li R, Liu Q (2006) Tower mast of precipitation over the central Tibetan Plateau summer. *Geophys Res Lett* 33:L05802. <https://doi.org/10.1029/2005GL024713>
- Gao W, Sui C, Fan J, Hu Z, Zhong L (2016) A study of cloud microphysics and precipitation over the Tibetan Plateau by radar observations and cloud-resolving model simulations. *J Geophys Res Atmos* 121:13735–13752. <https://doi.org/10.1002/2015jd024196>
- Gerken T, Biermann T, Babel W, Herzog M, Ma YM, Foken T, Graf HF (2013) A modelling investigation into lake-breeze development and convection triggering in the Nam Co Lake basin. *Tibetan Plateau Theor Appl Climatol* 117(1–2):149–167. <https://doi.org/10.1007/s00704-013-0987-9>
- Grell GA, Devenyi D (2002) A generalized approach to parameterizing convection combining ensemble and data assimilation techniques. *Geophys Res Lett*. <https://doi.org/10.1029/2002gl015311>
- Gu HP, Jin JM, Wu YH, EK MB, Subin ZM (2015) Calibration and validation of lake surface temperature simulations with the coupled WRF-lake model. *Clim Chang* 129:471–483. <https://doi.org/10.1007/s10584-013-0978-y>
- Gu HP, Jin JM, Wu YH, EK MB, Subin ZM, Ma ZG, Li MX (2016) Effect of a large and very shallow lake on local summer precipitation over the Lake Taihu basin in China. *J Geophys Res Atmos* 121:8832–8848. <https://doi.org/10.1002/2015jd024098>
- Gula J, Peltier WR (2012) Dynamical downscaling over the Great Lakes basin of North America using the WRF Regional Climate Model: the impact of the Great Lakes system on regional greenhouse warming. *J Clim* 25:7723–7742. <https://doi.org/10.1175/JCLI-D-11-00388.1>
- Haginoya S, Fujii H, Kuwagata T, Xu JQ, Ishigooka Y, Kang SC, Zhang YJ (2009) Air-lake interaction features found in heat and water exchanges over nam co on the Tibetan Plateau. *SOLA* 5:172–175. <https://doi.org/10.2151/sola.2009-044>
- Hong SY, Noh Y, Dudhia J (2006a) A new vertical diffusion package with an explicit treatment of entrainment processes. *Mon Weather Rev* 134:2318–2341. <https://doi.org/10.1175/MWR3199.1>
- Hong SY, Noh Y, Dudhia J, Lim JOJ (2006b) The WRF single-moment 6-class microphysics scheme (WSM6). *Asia Pac J Atmos Sci* 42:129–151
- Hostetler SW, Bates GT, Giorgi F (1993) Interactive coupling of a lake thermal model with a regional climate model. *J Geophys Res* 98:5045–5057. <https://doi.org/10.1029/92JD02843>
- Hostetler SW, Bates GT, Giorgi F, Giorgi F, Bates GT, Bartlein PJ (1994) Lake-atmosphere feedbacks associated with paleolakes Bonneville and Lahontan. *Science* 263:665–668. <https://doi.org/10.1126/science.263.5147.665>
- Huang AN, Zhao Y, Zhou Y, Yang B, Zhang LJ, Dong XN, Fang DX, Wu Y (2016) Evaluation of multisatellite precipitation products by use of ground-based data over China. *J Geophys Res Atmos* 121(10):654–675. <https://doi.org/10.1002/2016JD025456>
- Huffman GJ, Bolvin DT, Nelkin EJ, Wolff DB, Adler RF, Gu G, Hong Y, Bowman KP, Stocker EF (2007) The TRMM multisatellite precipitation analysis (TMPA): Quasi-global, multiyear, combined-sensor precipitation estimates at fine scales. *J Hydrometeorol* 8:38–55. <https://doi.org/10.1175/JHM560.1>
- Kourzeneva E (2010) External data for lake parameterization in numerical weather prediction and climate modeling. *Boreal Environ Res* 15:165–177
- Kourzeneva E, Asensio H, Martin E, Faroux S (2012) Global gridded dataset of lake coverage and lake depth for use in numerical weather prediction and climate modelling. *Tellus A* 64:15640. <https://doi.org/10.3402/tellusa.v64i0.15640>
- Krinner G (2003) Impact of lakes and wetlands on boreal climate. *J Geophys Res*. <https://doi.org/10.1029/2002jd002597>
- Lazhu, Yang K, Wang JB, Lei YB, Chen YY, Zhu LP, Ding BH, Qin J (2016) Quantifying evaporation and its decadal change for Lake Nam Co, central Tibetan Plateau. *J Geophys Res* 121:7578–7591. <https://doi.org/10.1002/2015JD024523>
- Lei YB, Yang K, Wang B, Sheng YW, Bird BW, Zhang GQ, Tian LD (2014) Response of inland lake dynamics over the Tibetan Plateau to climate change. *Clim Chang* 125:281–290. <https://doi.org/10.1007/s10584-014-1175-3>
- Li ZG, Lyu SH, Ao YH, Wen LJ, Zhao L, Wang SY (2015) Long-term energy flux and radiation balance observations over Lake Ngoring, Tibetan Plateau. *Atmos Res* 155:13–25. <https://doi.org/10.1016/j.atmosres.2014.11.019>
- Liu XB, Yao TD, Kang SC, Jiao NZ, Zeng YH, Liu YQ (2010) Bacterial community of the largest Oligosaline Lake, Namco on the Tibetan Plateau. *Geomicrobiol J* 27(8):669–682. <https://doi.org/10.1080/01490450903528000>
- Liao JJ, Shen GZ, Li YK (2013) Lake variations in response to climate change in the Tibetan Plateau in the past 40 years. *Int J Digit Earth* 534:549. <https://doi.org/10.1080/17538947.2012.656290>

- Lofgren BM (1997) Simulated effects of idealized Laurentian Great Lakes on regional and large-scale climate. *J. Climate* 10:2847–2858. [https://doi.org/10.1175/1520-0442\(1997\)010%3c284:SEOILG%3e2.0.CO;2](https://doi.org/10.1175/1520-0442(1997)010%3c284:SEOILG%3e2.0.CO;2)
- Long ZG, Perrie W, Gyakum J, Caya D, Laprise R (2007) Northern lake impacts on local seasonal climate. *J Hydrometeorol* 8(4):881–896. <https://doi.org/10.1175/JHM591.1>
- Lu SL, Jia L, Zhang L, Wei TP, Baig MHA, Zhai ZK, Meng JH, Li XS, Zhang GH (2017) Lake water surface mapping in the Tibetan Plateau using the MODIS MOD09Q1 product. *Remote Sens Lett* 8(3):224–233. <https://doi.org/10.1080/2150704X.2016.1260178>
- Lv YQ, Yang XY, Ma YM (2007) Numerical simulation of summer circulation and atmospheric boundary layer characteristics over qinghai lake. *Plateau Meteorol* 26(4):686–692
- Lv YQ, Yang XY, Ma YM, Li MS, Sun FL (2008) Study on characteristic of atmospheric boundary layer over lake namco region, Tibetan Plateau. *Plateau Meteorol* 27(6):1205–1210
- Ma YM, Han CB, Zhong L, Wang BB, Zhu ZK, Wang YJ, Zhang L, Meng CC, Xu C, Amatya PM (2014) Using MODIS and AVHRR data to determine regional surface heating field and heat flux distributions over the heterogeneous landscape of the Tibetan Plateau. *Theor Appl Climatol* 117:643–652. <https://doi.org/10.1007/s00704-013-1035-5>
- MacCallum SNCJ, Merchant (2012) Surface water temperature observations of large lakes by optimal estimation. *Remote Sens* 38(1):25–45. <https://doi.org/10.5589/m12-010>
- Martynov A, Sushama L, Laprise R, Winger K, Dugas B (2012) Interactive lakes in the canadian regional climate model, version 5: the role of lakes in the regional climate of North America. *Tellus* 64A:16226. <https://doi.org/10.3402/tellusa.v64i0.16226>
- Maussion F, Scherer D, Molg T, Collier E, Curio J, Finkelnburg R (2013) Precipitation seasonality and variability over the Tibetan Plateau as resolved by the high Asia reanalysis. *J Climate* 27:1910–1927. <https://doi.org/10.1175/JCLI-D-13-00282.1>
- Mironov D, Heise E, Kourzeneva E, Ritter B, Scgneider N, Terzhevik A (2010) Implementation of the lake parameterisation scheme FLake into the numerical weather prediction model COSMO. *Boreal. Environ Res* 15:218–230
- Mitchell K, Mike EK, Vince W, Dag L, Paul R (2005) The community noah land-surface model (LSM). In user's guide public release version 2.7.1. <ftp://ftp.emc.ncep.noaa.gov/mmb/gcp/ldas/noahls/sm/ver2.7.1>
- Mlawer EJ, Taubman SJ, Brown PD, Iacono MJ, Clough SA (1997) Radiative transfer for inhomogeneous atmospheres: RRTM, a validated correlated-k model for the longwave. *J Geophys Res* 102(D14):16663–16682. <https://doi.org/10.1029/97jd00237>
- NCEP/NOAA (2000) NCEP FNL operational model global tropospheric analyses, continuing from July 1999 (updated daily). NCAR Comput Inf Syst Lab Res Data Arch 1:1. <https://doi.org/10.5065/d6m043c6>
- Nordbo A, Launiainen S, Mammarella I, Lepparanta M, Huotari J, Ojala A, Vesala T (2011) Long-term energy flux measurements and energy balance over a small boreal lake using eddy covariance technique. *J Geophys Res.* <https://doi.org/10.1029/2010jd014542>
- Notaro M, Holman K, Zarrin A, Fluck E, Vavrus S, Bennington V (2013) Influence of the Laurentian Great Lakes on regional climate. *J. Climate* 26:789–804. <https://doi.org/10.1175/JCLI-D-12-00140.1>
- Oleson KW, Lawrence DM, Bonan GB, Drewniak B, Huang MY, Koven CD, Yang ZL (2013) Technical description of version 4.5 of the community land model (CLM). NCAR technical note NCAR/TN-503 + STR, National Center for Atmospheric Research, Boulder, pp. 422 <https://doi.org/10.5065/d6rr1w7m>
- Pereira G, Muscato M (2013) Multivariate analysis of lake-effect snowstorms in western New York. *J Operational Meteor* 1(14):157–167. <https://doi.org/10.15191/nwajom.2013.0114>
- Phan VH, Lindenbergh R, Menenti M (2012) ICESat derived elevation changes of Tibetan lakes between 2003 and 2009. *Int J Appl Earth Obs Geoinf* 17:12–22. <https://doi.org/10.1016/j.jag.2011.09.015>
- Ruthrich F, Reudenbach C, Thies B, Bendix J (2015) Lake-related cloud dynamics on the Tibetan Plateau: spatial patterns and inter-annual variability. *J Clim* 28:9080–9104. <https://doi.org/10.1175/JCLI-D-14-00698.1>
- Samuelsson P, Kourzeneva E, Mironov D (2010) The impact of lakes on the European climate as simulated by a regional climate model. *Boreal Environ Res* 15(2):113–129
- Shepard D (1968) A two-dimensional interpolation function for irregularly-spaced data. Proceedings of the 1968 ACM national conference, 27–29 August 1968, New York, pp 517–524. <https://doi.org/10.1145/800186.810616>
- Simmons AS, Uppala S, Dee D, Kobayashi S (2007) ERA-interim: new ECMWF reanalysis products from 1989 onwards. *ECMWF Newsltt* 110:25–35. <https://doi.org/10.21957/pocnrx23c6>
- Skamarock WC, Klemp JB, Dudhia J, Gill DO, Barker DM, Duda MG, Huang XY, Wang W, Powers JG (2008) A description of the advanced research WRF Version 3. NCAR technical note NCAR/TN-475 + STR. <https://doi.org/10.5065/d68s4mjh>
- Song CQ, Huang B, Ke LH (2014) Inter-annual changes of alpine inland lake water storage on the Tibetan Plateau, detection and analysis by integrating satellite altimetry and optical imagery. *Hydrol Process* 28(4):2411–2418. <https://doi.org/10.1002/hyp.9798>
- Stepanenko VM, Joehnk KD, Maxhulskaia E, Perroud M, Subin M, Nordbo A, Mammarella I, Mironov D (2014) Simulation of surface energy fluxes and stratification of a small boreal lake by a set of one-dimensional models. *Tellus A Dyn Meteorol Oceanogr* 66(1):21389. <https://doi.org/10.3402/tellusa.v66.21389>
- Su FG, Duan XL, Chen DL, Hao ZC, Cuo L (2013) Evaluation of the global climate models in the CMIP5 over the Tibetan Plateau. *J Clim* 26:3187–3208. <https://doi.org/10.1175/JCLI-D-12-00321.1>
- Subin ZM, Riley WJ, Mironov D (2012) An improved lake model for climate simulations: model structure, evaluation, and sensitivity analyses in CESM1. *J Adv Model Earth Syst* 4:M02001. <https://doi.org/10.1029/2011MS000072>
- Taylor KE (2001) Summarizing multiple aspects of model performance in a single diagram. *J Geophys Res* 106:7183–7192. <https://doi.org/10.1029/2000JD900719>
- Theeuwes NE, Steeneveld GJ, Krieken F, Holtslag AAM (2010) Mesoscale modeling of lake effect snow over Lake Erie—Sensitivity to convection, microphysics and the water temperature. *Adv Sci Res* 4:15–22. <https://doi.org/10.5194/asr-4-15-2010>
- Thiebaut J, Rogers E, Wang WQ, Katz B (2003) A new high-resolution blended real-time global sea surface temperature analysis. *Bull Am Meteor Soc* 84:645–656. <https://doi.org/10.1175/BAMS-84-5-645>
- Thiery W, Martynov A, Darchambeau F, Descy JP, Plisnie PD, Sushama L, Lipzig NPM (2014) Understanding the performance of the FLake model over two African Great Lakes. *Geosci Model Dev* 7:317–337. <https://doi.org/10.5194/gmd-7-317-2014>
- Thiery W, Martynov A, Darchambeau F, Descy JP, Plisnie PD, Sushama L, Lipzig NPM, Davin EL, Panitz HJ, Demuzere M, Lhermitte S, Lipzig NV (2015) The impact of the African great lakes on the regional climate. *J Clim* 28:4061–4085. <https://doi.org/10.1175/JCLI-D-14-00565.1>
- Vavrus S, Notaro M, Zarrin A (2013) The role of ice cover in heavy lake-effect snowstorms over the Great Lakes Basin as simulated by RegCM4. *Mon Weather Rev* 141(1):148–165. <https://doi.org/10.1175/MWR-D-12-00107.1>
- Verburg P, Antenucci JP (2010) Persistent unstable atmospheric boundary layer enhances sensible and latent heat loss in a tropical great lake: Lake Tanganyika. *J Geophys Res* 115:5347. <https://doi.org/10.1029/2009JD012839>

- Verburga P, Hecky RE (2009) The physics of the warming of Lake Tanganyika by climate change. *Limnol Oceanogr* 54(6):2418–2430. https://doi.org/10.4319/lo.2009.54.6_part_2.2418
- Wang JB, Zhu LP, Daut G, Ju JT, Lin X, Wang Y, Zhen XL (2009) Investigation of bathymetry and water quality of Lake Nam Co, the largest lake on the central Tibetan Plateau. *Limnology* 10:149–158. <https://doi.org/10.1007/s10201-009-0266-8>
- Wang JB, Zhu LP, Daut G, Ju JT, Lin X, Wang Y, Zhen XL, Peng P, Ma Q, Zhu L (2010) Modern limnological features of Tangra Yumco and Zhari Namco, Tibetan Plateau. *J Lake Sci* 22:629–632
- Wang JB, Zhu LP, Daut G, Ju JT, Lin X, Wang Y, Zhen XL, Ma YM, Ma WQ, Su ZB (2017) Physical controls on half-hourly, daily, and monthly turbulent flux and energy budget over a high-altitude small lake on the Tibetan Plateau. *J Geophys Res* 122:2289–2303. <https://doi.org/10.1002/2016JD026109>
- Wen LJ, Nagabhatla N, Zhao L, Li ZG, Chen SQ (2015a) Impacts of salinity parameterizations on temperature simulation over and in a hypersaline lake. *Chin J Ocean Limnol* 33:790. <https://doi.org/10.1007/s00343-015-4153-3>
- Wen LJ, Nagabhatla N, Zhao L, Li ZG, Chen SQ, Lv SH, Li ZG, Zhao L, Nagabhatla N (2015b) Impact of two biggest lakes on local temperature and precipitation in the Yellow River source region of the Tibetan Plateau. *Adv Meteorol* 1:1. <https://doi.org/10.1155/2015/248031>
- Williams K, Chamberlain J, Buontempo C, Bain C (2015) Regional climate model performance in the Lake Victoria basin. *Clim Dyn* 44:1699–1713. <https://doi.org/10.1007/s00382-014-2201-x>
- Wu GX, Liu YM, He B, Bao Q, Duan AM, Jin FF (2012) Thermal controls on the Asian summer monsoon. *Sci Rep* 2:404. <https://doi.org/10.1038/srep00404>
- Wu Y, Huang AN, Huang DQ, Chen F, Yang B, Zhou Y, Fang DX, Zhang LJ, Wen LJ (2017) Diurnal variations of summer precipitation over the regions east to Tibetan Plateau. *Clim Dyn* 2:1–21. <https://doi.org/10.1007/s00382-017-4042-x>
- Xiao CL, Lofgren BM, Wang J, Chu PY (2016) Improving the lake scheme within a coupled WRF-lake model in the Laurentian Great Lakes. *J Adv Model Earth Syst* 8:1969–1985. <https://doi.org/10.1002/2016MS000717>
- Xu YW, Kang SC, Zhang YL, Zhang YJ (2011) A method for estimating the contribution of evaporative vapor from Nam Co to local atmospheric vapor based on stable isotopes of water bodies. *Chin Sci Bull* 56(14):1511–1517. <https://doi.org/10.1007/s11434-011-4467-2>
- Xu LJ, Liu HZ, Du Q, Wang L (2016) Evaluation of the WRF-lake model over a highland freshwater in southwest China. *J Geophys Res* 121:1. <https://doi.org/10.1002/2016jd025396>
- Xue PF, Pal JS, Ye XY, Lenters JD, Huang CF, Chu PY (2016) Improving the simulation of large lakes in regional climate modeling: two-way lake-atmosphere coupling with a 3D hydrodynamic model of the great lakes. *J Clim*. <https://doi.org/10.1175/jcli-d-16-0225.1>
- Xue YK, Ma YM, Li Q (2017) Land-climate interaction over the Tibetan Plateau. *Oxf Res Encycl Clim Sci* 1:1. <https://doi.org/10.1093/acrefore/9780190228620.013.592>
- Yanai M, Li CF, Song ZS (1992) Seasonal heating of the Tibetan Plateau and its effects on the evolution of the Asian summer monsoon. *J Meteorol Soc Jpn* 79:419–434. https://doi.org/10.2151/jmsj1965.70.1B_319
- Yeager KN, Steenburgh WJ, Alcott TI (2013) Contributions of lake-effect periods to the cool-season hydroclimate of the great salt lake basin. *J Appl Meteor Climatol* 52:341–362. <https://doi.org/10.1175/JAMC-D-12-077.1>
- Yu RC, Xu Y, Zhou TJ, Li J (2007) Relation between rainfall duration and diurnal variation in the warm season precipitation over central eastern China. *Geophys Res Lett* 34(13):173–180. <https://doi.org/10.1029/2007GL030315>
- Yu RC, Xu Y, Zhou TJ, Li J, Li J, Zhang Y, Chen HM (2015) Improvement of rainfall simulation on the steep edge of the Tibetan Plateau by using a finite-difference transport scheme in CAM5. *Clim Dyn* 45(9):2937–2948. <https://doi.org/10.1007/s00382-015-2515-3>
- Zhang GQ, Yao TD, Xie HJ, Zhang KX, Zhu FJ (2014) Lakes' state and abundance across the Tibetan Plateau. *Chin Sci Bull* 59(24):3010–3021. <https://doi.org/10.1007/s11434-014-0258-x>
- Zhang C, Tang QH, Chen DL (2017) Recent changes in the moisture source of precipitation over the Tibetan Plateau. *J Clim* 30(5):1. <https://doi.org/10.1175/jcli-d-15-0842.1>
- Zhao L, Jin JM, Wang SY, EK MB (2012) Integration of remote-sensing data with WRF to improve lake-effect precipitation simulations over the Great Lakes region. *J Geophys Res* 117:D09102. <https://doi.org/10.1029/2011JD016979>
- Zhou TJ, Yu RC, Chen HM, Dai A, Pan Y (2008) Summer precipitation frequency, intensity, and diurnal cycle over China: a comparison of satellite data with gauge observations. *J Clim* 21(2007):3997–4010. <https://doi.org/10.1175/2008JCLI2028SI>
- Zhu LJ, Jin JM, Liu X, Tian L, Zhang QH (2017) Simulations of the impact of lakes on local and regional climate over the Tibetan Plateau. *Atmos Ocean* 1:10. <https://doi.org/10.1080/07055900.2017.1401-524>

Publisher's Note Springer Nature remains neutral with regard to jurisdictional claims in published maps and institutional affiliations.